Master Dynamique des Structures,
Matériaux et Systèmes Couplés

Space-time finite elements methods in elastodynamics

Student:
Jonathan Baptista

Supervisor:
Dr. Mathias Legrand

Vibrations and Structural Dynamics Laboratory
Faculty of Engineering - McGill University

École Centrale de Paris

Supméca

2010 - 2011

Contents

Résumé

Ce rapport parcourt différentes méthodes numériques utiles au traitement de la propagation d'ondes dans un milieu homogène avec, en arrière plan, une problématique d'impact. Une attention particulière est portée aux phénomènes numériques conduisant à une propagation d'ondes à vitesse infinie. Après un bref rappel des solutions théoriques pour une barre encastrée, les méthodes d'intégration temporelle directe de Newmark et les formulations en éléments finis continus et discontinus de Galerkin exploitées sur des domaines espace-temps non séparés sont comparées pour différents types de chargement en déplacement. Les perspectives d'utilisation de chacune de ces méthodes concluent ce rapport. Entre autres, il est mis en évidence que l'utilisation de formulations faibles couplant espace et temps permet de rendre compte de la propagation à vitesse finie de l'infomation dans la barre. Enfin, l'utilisation de formulations de Galerkin discontinues offre des perspectives intéressantes dans le cas de systémes soumis à des chargements non réguliers.

Abstract

In this report, different numerical methods dedicated to the treatment of wave propagation in homogeneous media are investigated, with an underlying interest to impact problems. A particular attention is paid to numerical phenomena leading to wave propagation at infinite velocity. After a brief background on theoretical solutions for a clamped homogeneous rod, direct time integration Newmark methods and Galerkin continuous and discontinuous finite elements methods expressed in non-separated time-space domains are compared for various prescribed displacements. In the conclusion, perspectives for use of each of these methods is discussed. It is shown that coupled space-time finite element formulations properly described the traveling of information throught the rod at finite velocity. It is highlighted that the use of discontinuous Galerkin formulations provides interesting properties in the case of non-smooth loading.

Introduction

McGill University and the Structural Dynamics and Vibration laboratory

McGill University is based in Montréal, Canada, and is the oldest university of the city. Founded in 1821, it is nowadays one of the best-known institutions of higher education in the country: ranked among the top 20 universities worldwide, it gathers over 36,000 students from more than 150 countries.

As for the research, McGill is ranked as one of the top research-intensive universities of the country, working in both fundamental and applied sciences, it has made significant contributions not only in health sciences, but also in engineering, computer sciences and social sciences.

Within the Faculty of Engineering, the *Structural Dynamics and Vibration Laboratory* is directed by Prof. Christophe Pierre and Dr. Mathias Legrand. The research carried out in this laboratory mainly focuses on nonlinear vibration, wave propagation, reduced-order models and linear and non-linear rotor dynamics, and is closely related to industrial needs in aeronautics.

Numerical methods in elastodynamics

Traditional numerical techniques involving finite element procedures for time-dependent phenomena assume a solution separated in time and space. For one-dimentional space problem, the sought solution takes the form $u(x,t) = N(x)U(t)$ where $u(x,t)$ stands for the displacement of a point x of the structure at time t. Such procedures are widely used in practice and well understood numerically. Through the derivation of finite elements in space, the original partial differential equations to be solved reduce to a system of ordinary differential equations in time which are, in turn, discretized by finite difference-like numerical schemes. The aforementioned technique leads to numerical difficulties because information of interest may propagate through the structures at infinite velocity. It is thought that non-separated space-time formulations could help circumventing this class of numerical difficulties. Such formulations require space-time domains of four dimensions when full three-dimensional structures are involved together with classical spatial boundary conditions and initial and final, if necessary, conditions.

Usually mechanical systems are macroscopically described by equations of continuum mechanics while discontnuities or sharp gradients in the sought

solution need a smaller scale to be accurately captured. In this line, several numerical approaches exist such as the multi-scale LArge Time INcrement (LATIN) method [4], the meshless Partition of Unity Finite Element Method [21] and the eXtented Finite Element Method [24].

This work focuses on the extension of classical finite element methods to periodic time-dependent systems with a particular emphasis on the space-time coupling and the treatment of potential jumps in the sought solution. First Newmark methods assuming separated space-time formulations are investigated. Then, non-separated space-time formulations and dedicated finite elements methods are introduced. Finally space-time discontinuous finite element methods are presented to address configurations involving discontinuities in the responses the mechanical systems of interest.

Chapter 1

Wave propagation in elastic structures

This chapter introduces the generic governing equations of motion and theoretical solutions for two physical systems of interest, solutions later employed for comparison purposes with the developped numerical strategies:

— a 1 degree-of-freedom (dof) spring-mass system;
— a 1 dimensional (1D) homogeneous elastic rod undergoing longitudinal travelling waves.

The aim of this chapter is also to present the notations and quantites of interest that will be later used throughout the document. It illustrates the difficulties implied by the propagation of information in elastic structures on two aspects:

— the smoothness of the travelling wave shape;
— the finite velocity of the travelling wave.

1.1 Preliminaries: a simple spring-mass system

First let us consider a one dof system consisting of a mass m and a spring k as illustrated in figure 1.1. This system is governed by the following equation of

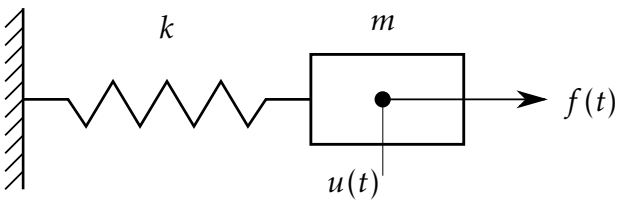

Figure 1.1: Spring mass system

motion together with the prescribed initial conditions:

$$\begin{aligned} \forall t \in]0;+\infty[, \quad & m\ddot{u}(t) + ku(t) = f(t) \\ & u(0) = u_0 \\ & \dot{u}(0) = v_0 \end{aligned} \tag{1.1}$$

When $f(t) = 0$, the exact solution is given by:

$$\forall t \in [0;+\infty[, \quad u(t) = u_0 \cos(\omega t) + \frac{v_0}{\omega}\sin(\omega t) \quad \text{with} \quad \omega = \sqrt{\frac{k}{m}} \tag{1.2}$$

Obviously, no wave can propagate in such a system. It nevertheless offers a quite simple analytical solution very useful for comparison with numerical results.

1.2 Generic wave equation

1.2.1 Longitudinal wave equation for infinite rod

In the context of the theory of small perturbations theory and when the external forcing g as well as the body force f_v are neglected, the behaviour of the elastic rod is completely described by the following equations:

$$\begin{aligned} \forall (x,t) \in \mathbb{R}\times]0;+\infty[, \quad & \frac{\partial^2 u}{\partial t^2}(x,t) - c^2 \frac{\partial^2 u}{\partial x^2}(x,t) = 0 \quad \text{with} \quad c = \sqrt{\frac{E}{\rho}} \\ \forall x \in \mathbb{R}, \quad & u(x,0) = u_0(x) \\ \forall x \in \mathbb{R}, \quad & \frac{\partial u}{\partial t}(x,0) = v_0(x) \end{aligned} \tag{1.3}$$

The explicit solution of this system of equations is known to be [6, p. 10]:

$$u(x,t) = \frac{1}{2}\Big(u_0(x-ct) + u_0(x+ct)\Big) + \frac{1}{2c}\int_{x-ct}^{x+ct} v_0(s)ds \tag{1.4}$$

Assuming $v_0 = 0$, the solution is the superimposition of two harmonic waves moving in opposite directions at velocity c. Figure 1.2 represents solution (1.4) for an initial window u_0 by families of lines of equation $x + ct = \text{cst}$ and $x - ct = \text{cst}$ starting from the initial condition u_0 in the space-time plane and called characteristic lines.

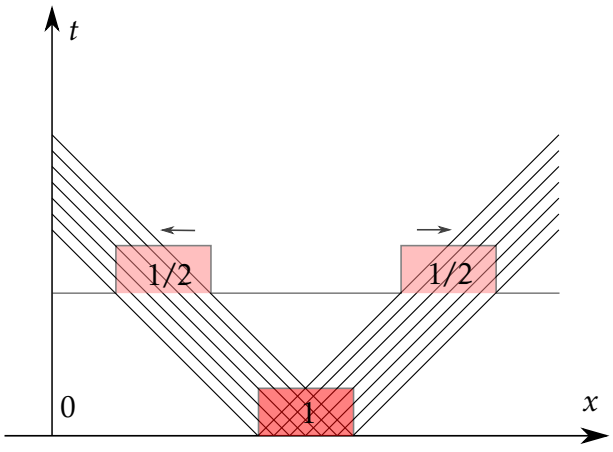

Figure 1.2: Solution of the wave equation for an infinite rod

1.2.2 Longitudinal wave equation for finite rod

The second investigated system is a one-dimensional homogeneous elastic rod depicted in figure 1.3 and undergoing an external forcing load $g(t)$ at the free end and a body force $\vec{f_v} = f_v \cdot \vec{x}$. The rod is of lenght L and cross-section area S, with a Young modulus E and a mass density ρ. It is clamped at $x = 0$. The

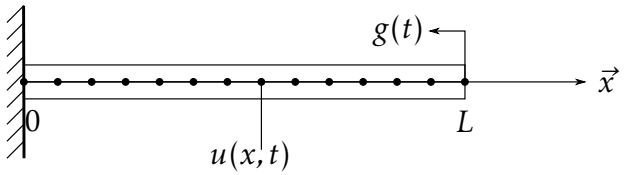

Figure 1.3: One-dimensional elastic rod

space domain is restricted to the interval $[0;L]$ such that (1.3) becomes:

$$\begin{aligned}
\forall (x,t) \in [0,L]\times]0;+\infty[, \quad & \frac{\partial^2 u}{\partial t^2}(x,t) - c^2 \frac{\partial^2 u}{\partial x^2}(x,t) = 0 \\
\forall t \in [0;+\infty[, \quad & u(0,t) = 0 \\
\forall t \in [0;+\infty[, \quad & \frac{\partial u}{\partial x}(L,t) = 0 \\
\forall x \in [0,L], \quad & u(x,0) = u_0(x) \\
\forall x \in [0,L], \quad & \frac{\partial u}{\partial t}(x,0) = v_0(x)
\end{aligned} \tag{1.5}$$

Assuming $v_0(x) = 0$, and knowing that the boundary conditions yield anti-symetry of solution (1.4) in $x = 0$ and symetry in $x = L$, a periodic solution is found: a portion of it is illustrated in figure 1.4 which shows the reflexions undergone by the initial window $u_0(x)$.

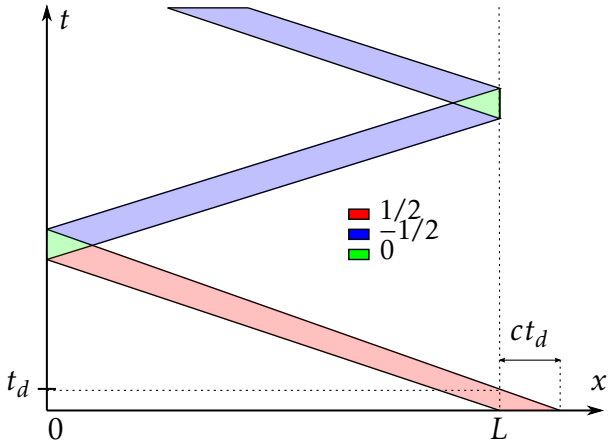

Figure 1.4: Solution of the wave equation for a finite rod

1.3 Impact boundary condition

In order to approximate a contact occurring at the free end of the rod, a displacement impulse is introduced at this point. This is reflected by a ramp

entry with a finite slope as depicted in figure 1.5(a). When the slope tends to infinity as displayed in figure 1.5(b), very sharp gradients in the solution may be expected. Of high interest is the development of numerical strategies able to address such non-differentiable entries.

It is assumed that the solution has two phases:

1. A first phase where displacement is prescribed: $u(L,t) = u_c(t)$, corresponding to impact/contact conditions, in red.
2. A second phase where the prescribed displacement is released: displacement of the tip of the rod is then free, in blue.

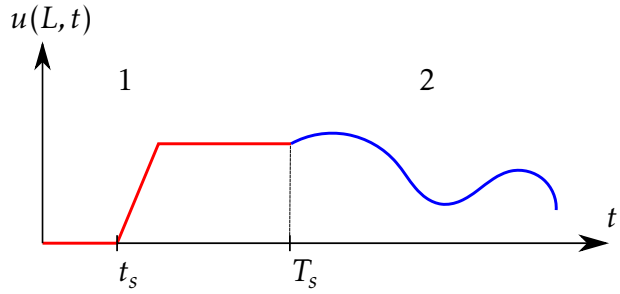

(a) with a finite slope

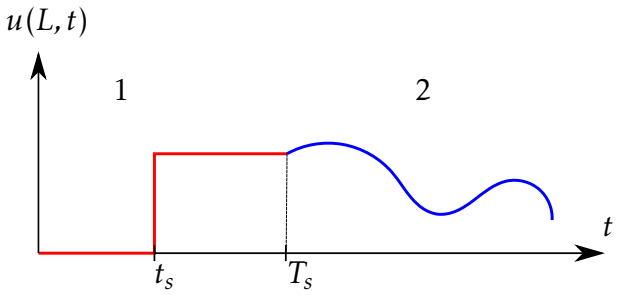

(b) with a infinite slope

Figure 1.5: Ramp entry

Such conditions are not exactly a displacement window as in section 1.2.2. These conditions correspond to a ramp followed by a constant step of displacement which then suddenly vanish. This case was studied in [19] and the respective graphical solution is shown in [22, p. 39]. The numerical solution for a finite slope is plotted in 3D in figure 2.2.

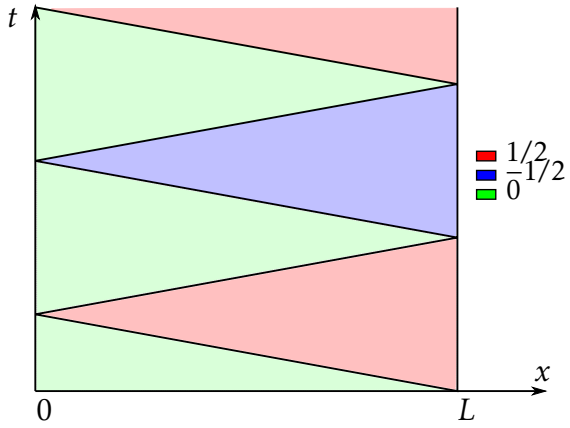

Figure 1.6: Solution of the wave equation to a ramp entry with an infinite slope for a finite rod

Chapter 2

Newmark schemes for elastodynamics

The Newmark family of time-integration methods is mainly employed for solving systems of, potentially nonlinear, ordinary differential equations. These schemes are easy to implement and sufficiently versatile to address a broad class of problems by seeking for a solution separated in time and space. This chapter is dedicated to their description in the context previously discussed. They will later be compared to more sophisticated solution methods.

2.1 Time integration schemes

2.1.1 Formulation

Consider the following system of second order differential equations along with two respective initial conditions in displacement and velocity:

$$\begin{aligned} \forall t \in]0;+\infty[, \quad & \mathbf{M}\ddot{\mathbf{u}}(t) + \mathbf{C}\dot{\mathbf{u}}(t) + \mathbf{K}\mathbf{u}(t) = \mathbf{f}(t) \\ & \mathbf{u}(0) = \mathbf{u}_0 \\ & \dot{\mathbf{u}}(0) = \mathbf{v}_0 \end{aligned} \tag{2.1}$$

These are the general settings used throughout the present report. Quantities $\mathbf{M}$, $\mathbf{C}$ and $\mathbf{K}$ are respectively the mass, the viscuous damping, and the stiffness matrices, obtained through the usual finite element approach detailed in section 2.3.1. Vector $\mathbf{f}$ stores the discretized external force and $\mathbf{u}$ is the displacement vector.

By assuming a time discretization such that $\mathbf{u}_n = \mathbf{u}(t_n) = \mathbf{u}(n\Delta t)$ where Δt stands as the constant time-step, equation (2.1) reads:

$$\begin{aligned} \forall n \in \mathbb{N}^{+*}, \quad & \mathbf{M}\mathbf{a}_n + \mathbf{C}\mathbf{v}_n + \mathbf{K}\mathbf{u}_n = \mathbf{f}_n \\ & \mathbf{u}(0) = \mathbf{u}_0 \\ & \dot{\mathbf{u}}(0) = \mathbf{v}_0 \end{aligned} \tag{2.2}$$

where the notations $\mathbf{a}_n = \ddot{\mathbf{u}}_n$ and $\mathbf{v}_n = \dot{\mathbf{u}}_n$ are used. By exploiting Taylor expansion theorem, displacement $\mathbf{u}_n$, velocity $\mathbf{v}_n$ and acceleration $\mathbf{a}_n$ can be expressed

with respect to their first time derivatives for each time step as follows:

$$\begin{aligned}
\mathbf{u}_{n+1} &= \mathbf{u}_n + \Delta t \mathbf{v}_n + \frac{\Delta t^2}{2}\mathbf{a}_{n+2\beta} \\
\mathbf{v}_{n+1} &= \mathbf{v}_n + \Delta t \mathbf{a}_{n+\gamma} \\
\mathbf{a}_{n+2\beta} &= (1-2\beta)\mathbf{a}_n + 2\beta \mathbf{a}_{n+1} \\
\mathbf{a}_{n+\gamma} &= (1-\gamma)\mathbf{a}_n + \gamma \mathbf{a}_{n+1}
\end{aligned} \tag{2.3}$$

where β and γ are user-defined constants as detailed in section 2.1.3.

2.1.2 Implementation

Equations (2.2) and (2.3) are combined so that time-integration algorithm 1 can be implemented. It involves quantities $\mathbf{u}^p_{n+1}$ and $\mathbf{v}^p_{n+1}$ which are the predictor terms depending on the previous time step n [12].

Algorithm 1 Newmark time integration scheme

Require: γ, β
Require: Initial conditions: $\mathbf{u}_0$, $\mathbf{v}_0$
  $\mathbf{a}_0 \leftarrow (\mathbf{M} + \gamma\Delta t\mathbf{C} + \beta\Delta t^2\mathbf{K})^{-1}(\mathbf{f}_0 - \mathbf{C}\mathbf{v}_0 - \mathbf{K}\mathbf{u}_0)$
  for $n = 0$ **to** N **do**
    $\mathbf{u}^p_{n+1} \leftarrow \mathbf{u}_n + \Delta t\mathbf{v}_n + \frac{\Delta t^2}{2}(1-2\beta)\mathbf{a}_n$
    $\mathbf{v}^p_{n+1} \leftarrow \mathbf{v}_n + \Delta t(1-\gamma)\mathbf{a}_n$
    $\mathbf{a}_{n+1} \leftarrow (\mathbf{M} + \gamma\Delta t\mathbf{C} + \beta\Delta t^2\mathbf{K})^{-1}(\mathbf{f}_{n+1} - \mathbf{C}\mathbf{v}^p_{n+1} - \mathbf{K}\mathbf{u}^p_{n+1})$
    $\mathbf{u}_{n+1} \leftarrow \mathbf{u}^p_{n+1} + \Delta t^2\beta\mathbf{a}_{n+1}$
    $\mathbf{v}_{n+1} \leftarrow \mathbf{v}^p_{n+1} + \gamma\Delta t\mathbf{a}_{n+1}$
  end for

Any system of second-order differential equation can be recasted in a system of first-order differential equation. When generalized to the n^{th} time step through an amplification matrix $\mathbf{A}$, the displacement and velocity at time t_n are related to the initial displacement and velocity as follows:

$$\forall n \in \mathbb{N}^{+*}, \quad \begin{pmatrix}\mathbf{u}_n \\ \mathbf{v}_n\end{pmatrix} = \mathbf{A}^n \begin{pmatrix}\mathbf{u}_0 \\ \mathbf{v}_0\end{pmatrix} \tag{2.4}$$

An eigenvalue analysis of matrix $\mathbf{A}$ provides information about the stability of the method. In order to be stable, the magnitude of the eigenvalues of $\mathbf{A}$ must be smaller than unity.

2.1.3 Numerical properties

As already mentioned, Newmark schemes depend on coefficients γ and β. These two coefficients drive the numerical properties of the underlying solution method: it can be either *explicit* or *implicit* and *conditionally* or *unconditionally* stable. The most common combinations are summarized in table 2.1. Stability conditions are well define in literature [7] for this type of numerical schemes.

Method	γ	β	Stability
Central Differences	1/2	0	explicit and conditionally stable
Fox-Goodwin	1/2	1/12	implicit and conditionally stable
Linear acceleration	1/2	1/6	implicit and conditionally stable
Average acceleration	1/2	1/4	implicit and unconditionally stable

Table 2.1: Parameters γ and β in Newmark Schemes

Newmark schemes are unstable for $\gamma \leq 1/2$, unconditionally stable for $1/2 \leq \gamma \leq 2\beta$ and conditionally stable if $1/2 \leq \gamma$ and $2\beta \leq \gamma$ (under a condition combining time step and spatial mesh size, see 3.2.3). Moreover for $\gamma = 1/2$, Newmark method is second order accurate and this is the reason why this value is often assigned to γ. When $\beta = 0$, the scheme is explicit.

Integration Method order Consider ψ, the numerical solution such that $\psi_n = \psi(t_n)$ and y, the exact solution known and given in 1.1 for a spring-mass system. One can define δ_n the local error over one step of the integration method by:

$$\forall n \in [\![0, N]\!] \quad \delta_n = \psi_n - y(t_n) \tag{2.5}$$

and $\delta_{\max}$ the global error by:

$$\delta_{\max} = \max_{n \in [\![0,N]\!]} (\delta_n) = \max_{n \in [\![0,N]\!]} \Big(\psi(t_n) - y(t_n) \Big) \tag{2.6}$$

The method is said to be of order p if $\delta_n = \mathcal{O}(\Delta t^{p+1})$ or if $\delta_{\max} = \mathcal{O}(\Delta t^p)$ when $\Delta t \to 0$.

2.2 Simple spring-mass system

2.2.1 Central differences scheme

Equation (1.1) is now investigated through a finite central difference integration approach:

$$a_n + \omega^2 u_n = 0 \tag{2.7}$$

One can refer to equation (2.2) by considering scalars m and k as the 1-by-1 matrices $\mathbf{M}$ and $\mathbf{K}$, and $\mathbf{C} = \mathbf{0}$. On a finite time interval $[0, T]$, Newmark method with the proper β and γ parameters yields:

$$a_n = \frac{u_{n+1} - 2u_n + u_{n-1}}{\Delta t^2} \tag{2.8}$$

and the discretized equation to be solved reads:

$$\forall n \in [\![0, N]\!], \quad b u_{n+1} + 2a u_n + b u_{n-1} = 0 \tag{2.9}$$

with $2a = 1/\Delta t^2$ and $b = \omega^2 - 2/\Delta t^2$, which is equivalent to the following linear system:

$$\begin{pmatrix} 1 & 0 & \cdots & \cdots & 0 \\ -1 & 1 & \ddots & & \vdots \\ b & 2a & b & \ddots & \vdots \\ \vdots & \ddots & \ddots & \ddots & 0 \\ 0 & \cdots & b & 2a & b \end{pmatrix} \begin{pmatrix} u_1 \\ u_2 \\ \vdots \\ \\ u_{N+1} \end{pmatrix} = \begin{pmatrix} u_0 \\ \Delta t v_0 \\ \vdots \\ \\ f_{N+1} \end{pmatrix} \tag{2.10}$$

Solution method for linear system (2.10) is implemented in a new algorithm equivalent to algorithm 1 and detailed in section 3.1.2.

2.2.2 Error analysis

The spring-mass system used for the calculation over a period $T = 10$ s has the following properties: $m = 10$ kg, $k = 10$ N/m, $u_0 = 0.5$ m and $v_0 = -0.5$ m/s. Respective convergence rate of various Newmark schemes is depicted in figure 2.1. One can notice that implicite schemes provide the best results and

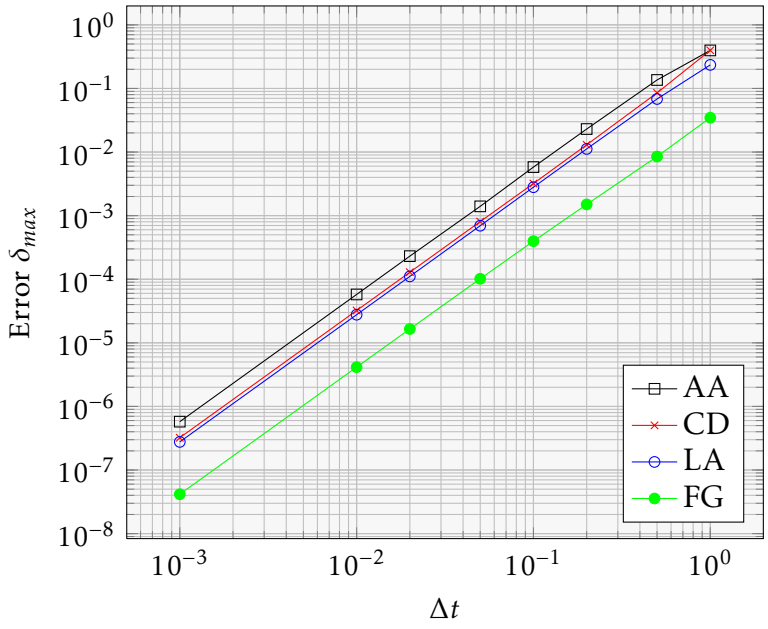

Figure 2.1: Convergence of the solution for Newmark schemes

particularly the Fox-Goodwin Newmark scheme (FG). Since methods are all second order accurate, their convergence rate features the same exponentiation: $\delta_{\max} \sim \Delta t^2$ when $\Delta t \to 0$.

2.3 Rod with time dependent boundary conditions

2.3.1 Formulation

The formulation for a n-DoF system is a little bit different since boundary conditions in space and time have to be dealt with.

Consider the rod described in 1.2 and whose displacement at its end is prescribed during a period T_c and then released. The governing equation (1.5) are modified as follows:

$$\begin{cases} \forall (x,t) \in [0,L]\times]0;+\infty[, & ES\dfrac{\partial^2 u}{\partial x^2}(x,t) + f_v = \rho S \dfrac{\partial^2 u}{\partial t^2}(x,t) \\ \forall t \in [0;+\infty[, & u(0,t) = 0 \\ \forall t \in [0;T_c[, & u(L,t) = u_c(t) \\ \forall t \in [T_c;+\infty[, & E\dfrac{\partial u}{\partial x}(L,t) = g(t) \\ \forall x \in [0,L], & u(x,0) = u_0(x) \\ \forall x \in [0,L], & \dfrac{\partial u}{\partial t}(x,0) = v_0(x) \end{cases} \tag{2.11}$$

Since displacement is released at the end of the *contact* period $[0;T_c[$, the potential external forcing acting at $x = L$ is zero, thus $g = 0$. In order to simplify calculations u_0, v_0 and f_v are all nill as well.

Then, the use of Newmark time integration scheme assumes a separtion between time and space in the sought solution 2.12. Space integration is realized through the Finite Element Method (FEM) while integration over time is performed through a numerical scheme detailed in section 2.1. Therefore, integration in space yields solutions of the form:

$$\begin{cases} \forall (x,t) \in [0,L]\times]0;+\infty[, & u(x,t) = \displaystyle\sum_{i=1}^{N_s} u_i(t) w_i(x) \\ \forall t \in [0;+\infty[, & u(0,t) = 0 \\ \forall t \in [0;T_c[, & u(L,t) = u_c(t) \end{cases} \tag{2.12}$$

The corresponding weak formulation is obtained by reporting $u(x,t)$ from (2.12) into the first equation of (2.11) and premultiplying by admissible trial functions $\psi_i \in \mathcal{C}_a = \{\psi \in H^1([0,L]),\ \psi(0) = 0\}$ such that: $\forall j \in [\![1,N_s]\!], \forall t \in]0;+\infty[$,

$$ES\sum_{i=1}^{N_s}\left(\int_0^L \frac{\partial w_i}{\partial x}\frac{\partial \psi_j}{\partial x}dx\right)u_i + \rho S\sum_{i=1}^{N_s}\left(\int_0^L w_i\psi_j dx\right)\frac{\partial^2 u_i}{\partial t^2} = Sg(t)\psi_j(L) \tag{2.13}$$

Remark 1 (Basis function in space)**.** *The condition $u(L,t) = u_c$ is not accounted for in $\mathcal{C}_a$ because this condition is time dependent while basis functions are not.*

2.3.2 Numerical scheme and implementation

Once again, one can refer to equation (2.2) by considering $N_s \times N_s$ matrices $\mathbf{M}$ and $\mathbf{K}$ define as follows: $\forall (i,j) \in [\![1,N_s]\!]^2$,

$$\mathbf{K}_{ij} = ES\int_0^L \frac{\partial w_i}{\partial x}\frac{\partial \psi_j}{\partial x}dx \qquad \mathbf{M}_{ij} = \rho S\int_0^L w_i\psi_j dx \tag{2.14}$$

These matrices are symmetric if $\psi_i = w_i$. Accordingly, linear trial functions in space are chosen. This formulation leads to solve equation (2.2) taking into account the clamped condition in $x = 0$ and the enforced displacement in $x = L$ by considering the following displacement vector $\mathbf{u}_n$ at time t_n:

$$\forall n \in \mathbb{N}^{+*}, \quad \mathbf{u}_n = \begin{pmatrix} u_n^1 = u_n(0) = 0 \\ \vdots \\ u_n^i \\ \vdots \\ u_n^{N_s} = u_n(L) = u_c \end{pmatrix} \tag{2.15}$$

The first component of vectors $\mathbf{u}_n$, $\mathbf{v}_n$ and $\mathbf{a}_n$ such as the first line and the first column of matrices $\mathbf{M}$, $\mathbf{C}$ and $\mathbf{K}$ have to be removed from system (2.2) which is now of size $N_s - 1$.

Vector $\mathbf{u}$ is then partitioned in $\mathbf{u}_1$ and $\mathbf{u}_2$, so are $\mathbf{v}$ and $\mathbf{a}$. Equation (2.2) writes $\forall n \in \mathbb{N}^{+*}$:

$$\begin{bmatrix} \mathbf{M}_{11} & \mathbf{M}_{12} \\ \mathbf{M}_{21} & \mathbf{M}_{22} \end{bmatrix} \begin{pmatrix} \mathbf{a}_{1n} \\ \mathbf{a}_{2n} \end{pmatrix} + \begin{bmatrix} \mathbf{C}_{11} & \mathbf{C}_{12} \\ \mathbf{C}_{21} & \mathbf{C}_{22} \end{bmatrix} \begin{pmatrix} \mathbf{v}_{1n} \\ \mathbf{v}_{2n} \end{pmatrix} + \begin{bmatrix} \mathbf{K}_{11} & \mathbf{K}_{12} \\ \mathbf{K}_{21} & \mathbf{K}_{22} \end{bmatrix} \begin{pmatrix} \mathbf{u}_{1n} \\ \mathbf{u}_{2n} \end{pmatrix} = \begin{pmatrix} \mathbf{f}_{1n} \\ \mathbf{f}_{2n} \end{pmatrix} \tag{2.16}$$

The first block in equation (2.16) provides the system behaviour while the second one provides the resultant force $\mathbf{f}_2$ due to the enforced displacement. Since the displacement is only enforced over a period T_c, algorithm 2 has to be implemented.

Algorithm 2 Newmark scheme with enforced/free displacement

Require: γ, β, u_c and Initial conditions: $\mathbf{u}_0$, $\mathbf{v}_0$

$\mathbf{u}_2 \leftarrow \mathbf{u}_c$; $\mathbf{v}_2 \leftarrow \dot{\mathbf{u}}_2$; $\mathbf{a}_2 \leftarrow \dot{\mathbf{v}}_2$

$\mathbf{a}_{10} \leftarrow (\mathbf{M}_{11} + \gamma\Delta t\mathbf{C}_{11} + \beta\Delta t^2\mathbf{K}_{11})^{-1}(\mathbf{f}_{10} - \mathbf{C}_{11}\mathbf{v}_{10} - \mathbf{K}_{11}\mathbf{u}_{10} - \mathbf{M}_{12}\mathbf{a}_{20} - \mathbf{C}_{12}\mathbf{v}_{20} - \mathbf{K}_{12}\mathbf{u}_{20})$

Enforced displacement phase

for $n = 0$ **to** N_{T_c} **do**

$\mathbf{u}_{1n+1}^p \leftarrow \mathbf{u}_{1n} + \Delta t\mathbf{v}_{1n} + \frac{\Delta t^2}{2}(1 - 2\beta)\mathbf{a}_{1n}$

$\mathbf{v}_{1n+1}^p \leftarrow \mathbf{v}_{1n} + \Delta t(1 - \gamma)\mathbf{a}_{1n}$

$\mathbf{a}_{1n+1} \leftarrow (\mathbf{M}_{11} + \gamma\Delta t\mathbf{C}_{11} + \beta\Delta t^2\mathbf{K}_{11})^{-1}(\mathbf{f}_{1n+1} - \mathbf{C}_{11}\mathbf{v}_{1n+1}^p - \mathbf{K}_{11}\mathbf{u}_{1n+1}^p - \mathbf{M}_{12}\mathbf{a}_{2n} - \mathbf{C}_{12}\mathbf{v}_{2n} - \mathbf{K}_{12}\mathbf{u}_{2n})$

$\mathbf{u}_{1n+1} \leftarrow \mathbf{u}_{1n+1}^p + \Delta t^2\beta\mathbf{a}_{1n+1}$

$\mathbf{v}_{1n+1} \leftarrow \mathbf{v}_{1n+1}^p + \gamma\Delta t\mathbf{a}_{1n+1}$

end for

Transition: $\mathbf{u}_{N_{T_c}} \leftarrow (\mathbf{u}_{1N_{T_c}}; \mathbf{u}_{2N_{T_c}})$; $\mathbf{v}_{N_{T_c}} \leftarrow (\mathbf{v}_{1N_{T_c}}; \mathbf{v}_{2N_{T_c}})$; $\mathbf{a}_{N_{T_c}} \leftarrow (\mathbf{a}_{1N_{T_c}}; \mathbf{a}_{2N_{T_c}})$

Free displacement phase:

for $n = N_{T_c}$ **to** N **do**

$\mathbf{u}_{n+1}^p \leftarrow \mathbf{u}_n + \Delta t\mathbf{v}_n + \frac{\Delta t^2}{2}(1 - 2\beta)\mathbf{a}_n$

$\mathbf{v}_{n+1}^p \leftarrow \mathbf{v}_n + \Delta t(1 - \gamma)\mathbf{a}_n$

$\mathbf{a}_{n+1} \leftarrow (\mathbf{M} + \gamma\Delta t\mathbf{C} + \beta\Delta t^2\mathbf{K})^{-1}(\mathbf{f}_{n+1} - \mathbf{C}\mathbf{v}_{n+1}^p - \mathbf{K}\mathbf{u}_{n+1}^p)$

$\mathbf{u}_{n+1} \leftarrow \mathbf{u}_{n+1}^p + \Delta t^2\beta\mathbf{a}_{n+1}$

$\mathbf{v}_{n+1} \leftarrow \mathbf{v}_{n+1}^p + \gamma\Delta t\mathbf{a}_{n+1}$

end for

2.3.3 Results

For the calculation, the structural damping $\mathbf{C}$ as well as g are neglected and $v_0 = 0$ is prescribed. The enforced displacement is a ramp at the free end of the rod $x = L$ at $t_s = 0.3$ s (see figure 1.5(a)). Then displacement and velocity are observed at $x = L/2$ with $\Delta t = 10^{-3}$ s and $\Delta x = L/30$ m. In figure 2.2, reponse

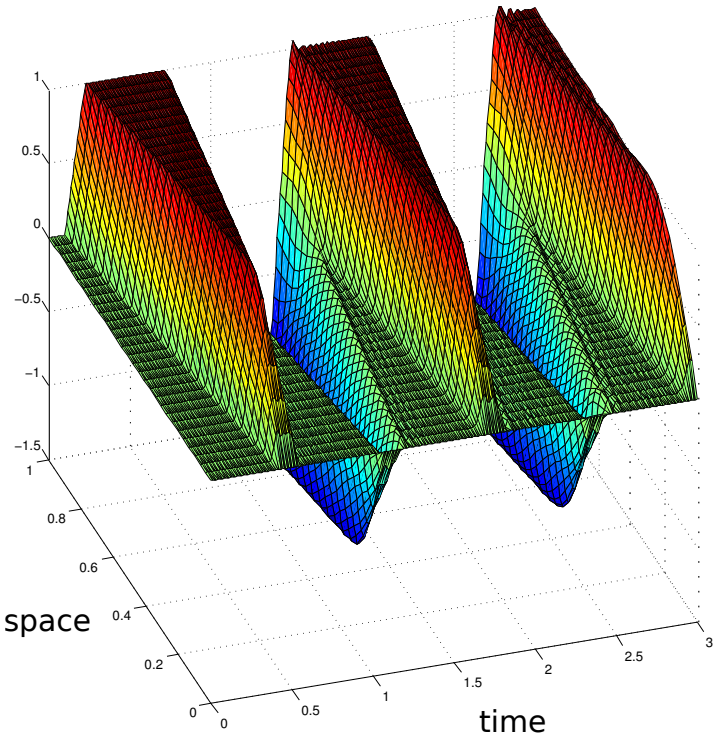

Figure 2.2: Solution for a finite ramp entry

to a ramp entry with $\Delta t = 10^{-2}$ s and $\Delta x = \frac{L}{30}$ is plotted. Later in this report, for more graphical convenience, results for the 1D case will be provided as cross-sections of this type of surfaces.

In section 2.1.3, implicit and explicit methods were introduced. Implicit methods usually require more demanding computational effort since solution at time t_{n+1} involves state of the sytem at time t_n and t_{n+1}. Nonetheless, they are usefull when explicit methods require impractically small time steps.

In the case of an explicit Newmark scheme without structural damping ($\mathbf{C} = \mathbf{0}$ and $\beta = 0$), the acceleration is computed as follows:

$$\mathbf{a}_{n+1} \leftarrow \mathbf{M}^{-1}(\mathbf{f}_{n+1} - \mathbf{K}\mathbf{u}^{p}_{n+1}) \tag{2.17}$$

However, the mass matrix $\mathbf{M}$ is not diagonal and propagates the information with an unbounded velocity into the discrete system. This inconsistency stems from the assumed separation of variable and can be avoided through lumping only. This is most of the time not a problem but can lead to numerical difficulties in very specific configurations.

In order to avoid this phenomena, one can choose to diagonalize the mass matrix. The effects of the so called lumped mass matrix [23] on the displacement are introduced in figure 2.3. It can be seen, for the first ramp at time

$t = t_s + \frac{L}{2c}$ that unlike consistant mass matrix, displacement at $x = L/2$ remains nil until the propagating wave reaches this point. It means that no information travels along the rod with an infinite speed and the respective displacement is in agreement with the theoretical solution exposed in 1.3. The lumped

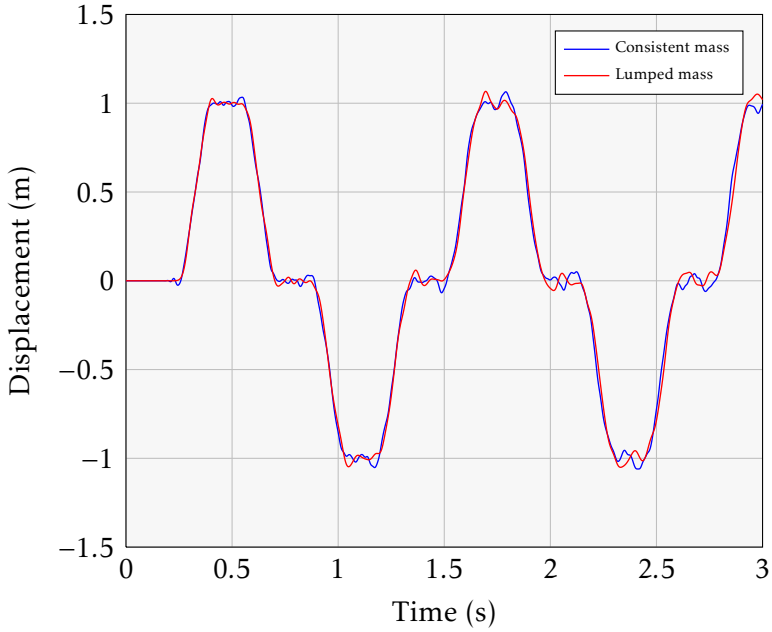

Figure 2.3: Displacement with central differences for a ramp entry at $x = L/2$

mass matrix also tends to soften the solution as illustrated on the velocity in figure 2.4. Also, high frequency oscillations around the theoretical solution

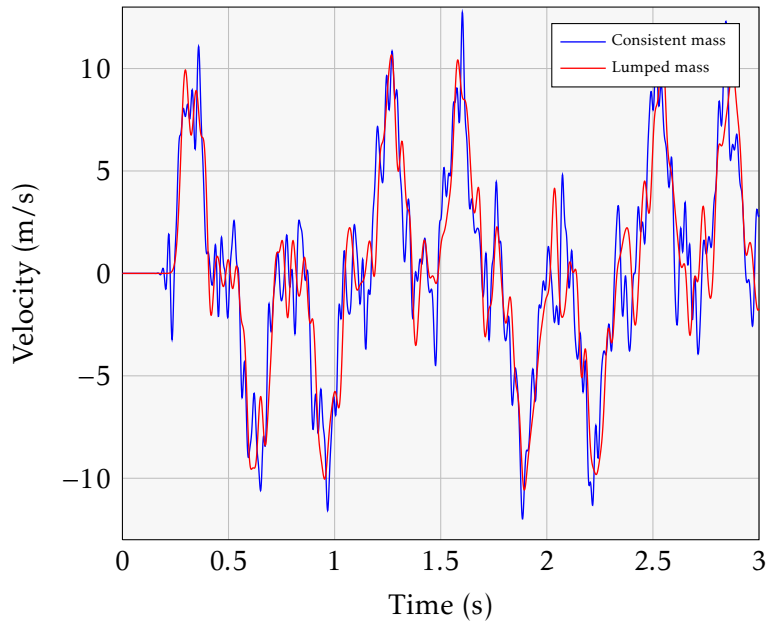

Figure 2.4: Velocity with central differences for a ramp entry at $x = L/2$

can be noticed. A way to partially dissipate them is to introduce a structural

damping which change the structural properties or to introduce a numerical damping as proposed by the generalized-α method [8, 9]. Such formulations may have undesirable effects and should sometimes be avoided.

Chapter 3

Continuous Galerkin Methods

A popular time integration scheme is detailed in chapter 2. The use of finite elements in space as well as in time is now of interest. This chapter is devoted to the extension of finite elements in space to the time domain by continuous space-time fonctions. Few works have been reported on the Space Time Continuous Finite Elements Method (STCFEM) also called Continuous Galerkin Method (CGM). The reader will find further information in [1, 2, 16, 18].

3.1 Time finite elements method

3.1.1 Formulation

Consider the 1DoF spring-mass system described in 1.1 with a time interval restricted to $[0,T]$:

$$\begin{cases} \forall t \in]0;T], & m\ddot{u}(t) + ku(t) = f(t) \\ & u(0) = u_0 \\ & \dot{u}(0) = v_0 \end{cases} \tag{3.1}$$

From (3.1), the weak formulation for the unknown u is:

$$\text{Find } u \in \mathcal{C}_a \text{ s.t. } \int_0^T (ku + m\ddot{u} - f)\psi \, dt = 0 \quad \forall \psi \in \mathcal{C} \tag{3.2}$$

with $\mathcal{C}_a = \{w \in H^1([0;T]),\ w(0) = u_0\}$ and $\mathcal{C} = H^1([0;T])$.

An integration by part of the acceleration term in equation (3.2) and assuming no discontinuities at $t = 0$ and $t = T$ yields:

$$\begin{aligned} &\text{Find } u \in \mathcal{C}_a \\ &\forall \psi \in \mathcal{C}, \quad \int_0^T (ku\psi - m\dot{u}\dot{\psi})\, dt + m\dot{u}(T)\psi(T) = \int_0^T f\psi \, dt + mv_0\psi(0) \end{aligned} \tag{3.3}$$

A regular time mesh of interval $[0,T]$ consisting in N subintervals $[t_{n-1}, t_n]$ for $n \in [\![1, N]\!]$ is considered to interpolate the displacement with linear basis functions in time $w_i(t)$:

$$\forall t \in [0;T], \quad u(t) = \sum_{i=1}^{N} u_i w_i(t) \tag{3.4}$$

The classical FEM is used to calculate the respective matrices and vectors: $\forall (i,j) \in [\![1,N]\!]^2$,

$$\begin{gathered}\mathbf{M}_{ij} = m\int_0^T \frac{dw_j}{dt}\frac{d\psi_i}{dt}\,dt \quad ; \quad \mathbf{K}_{ij} = k\int_0^T w_j\psi_i\,dt \quad ; \quad \mathbf{\Lambda}_{ij} = mw_j(T)\psi_i(T) \\ \mathbf{f}_i = k\int_0^T f\psi_i\,dt \quad ; \quad \lambda_{\mathbf{0}i} = mv_0\psi_i(0)\end{gathered} \tag{3.5}$$

Similarly to what was done in section 2.3.2, we choose $\psi_i(t) = w_i(t)$ in order to have symmetric matrices.

Remark 2 (Assembled matrices)**.** **M** *and* **K** *are the assembled mass and spring matrices, respectively. They have been built from the elementary mass and spring matrices.*

Other formulations are possible using the velocity v, strain or stress as unknown. According to [1], formulations limited to the displacement field give the best results. A two-field formulation using u and v for the continuous Galerkin method is described in [15]. Since we are mainly interested in the displacement field, the single-field displacement formulation was selected.

3.1.2 Numerical scheme for linear elements

Combining equations (3.3) and (3.5) yields the following discrete system of equations (3.6):

$$(\mathbf{K} - \mathbf{M} + \mathbf{\Lambda})\mathbf{u} = \mathbf{f} + \lambda_{\mathbf{0}} \quad \Leftrightarrow \quad \mathbf{R}\mathbf{u} = \mathbf{F} \tag{3.6}$$

where **u** is the discrete displacement vector consisting of displacement values at all time steps, **R** is the resultant matrix, and **F** stands as the generalized force vector. The vector **u** is of size $N+1$.

By construction, using linear functions and constant time steps, system (3.6) has the following structure:

$$\begin{pmatrix} a & b & 0 & \cdots & 0 \\ b & 2a & b & & \vdots \\ 0 & \ddots & \ddots & \ddots & 0 \\ \vdots & & b & 2a & b \\ 0 & \cdots & 0 & \lambda_1 & \lambda_2 \end{pmatrix} \begin{pmatrix} u_1 \\ \\ \vdots \\ \\ u_{N+1} \end{pmatrix} = \begin{pmatrix} f_1 + mv_0 \\ \\ \vdots \\ \\ F_{N+1} \end{pmatrix} \tag{3.7}$$

Since the first coordinates $u_1 = u_0$ is known, the first line of system 3.6 leads to:

$$u_2 = \frac{f_1 + mv_0 - au_1}{b} \tag{3.8}$$

The band structure of **R** allows for a simple iterative scheme to calculate the $(n+1)^{\text{th}}$ component of **u**. The last line of **R** is not useful when there is

no discontinuities at the final intant T. Accordingly, equation (3.7) can be reorganized as follows:

$$\begin{pmatrix} 1 & 0 & \cdots & \cdots & 0 \\ 0 & b & \ddots & & \vdots \\ b & 2a & b & \ddots & \vdots \\ \vdots & \ddots & \ddots & \ddots & 0 \\ 0 & \cdots & b & 2a & b \end{pmatrix} \begin{pmatrix} u_1 \\ u_2 \\ \vdots \\ \\ u_{N+1} \end{pmatrix} = \begin{pmatrix} u_0 \\ f_1 + mv_0 - au_0 \\ \vdots \\ \\ F_{N+1} \end{pmatrix} \tag{3.9}$$

System (3.9) is an explicit scheme similar to the central differences scheme (2.10) because a constant time-step is used. Instead of inverting very the large matrix $\mathbf{R}$ which becomes even larger when spatial dimension increases, algorithm 3 is preferred.

Algorithm 3 Continuous Galerkin with linear elements

Require: a, b and $\mathbf{f}$
Require: Initial conditions: $\mathbf{u}_0$, $\mathbf{v}_0$
  $u_1 \leftarrow u_0$
  $u_2 \leftarrow \frac{f_1 + mv_0 - au_0}{b}$
  for $n = 3$ **to** N **do**
    $u_n \leftarrow \frac{F_n - 2au_{n-1} - bu_{n-2}}{b}$
  end for

3.1.3 Numerical scheme for quadratic elements

For quadratic elements, assuming a constant time step Δt, one can use the three following basis functions:

$$w_1 = \frac{(t - t_n)(t - t_{n+1})}{2\Delta t^2} \quad ; \quad w_2 = 1 - \frac{(t - t_n)^2}{\Delta t^2} \quad ; \quad w_3 = \frac{(t - t_n)(t - t_{n-1})}{2\Delta t^2} \tag{3.10}$$

The respective elementary mass and stiffness matrices are defined as follows:

$$\mathbf{K_e} = \frac{k\Delta t}{15} \begin{pmatrix} 4 & 2 & -1 \\ 2 & 16 & 2 \\ -1 & 2 & 4 \end{pmatrix} \quad ; \quad \mathbf{M_e} = \frac{m}{6\Delta t} \begin{pmatrix} -7 & -8 & -2 \\ -4 & -8 & 4 \\ -2 & 4 & -7 \end{pmatrix} \tag{3.11}$$

By plugging the elementary matrices (3.11) into equation (3.6), system (3.7)

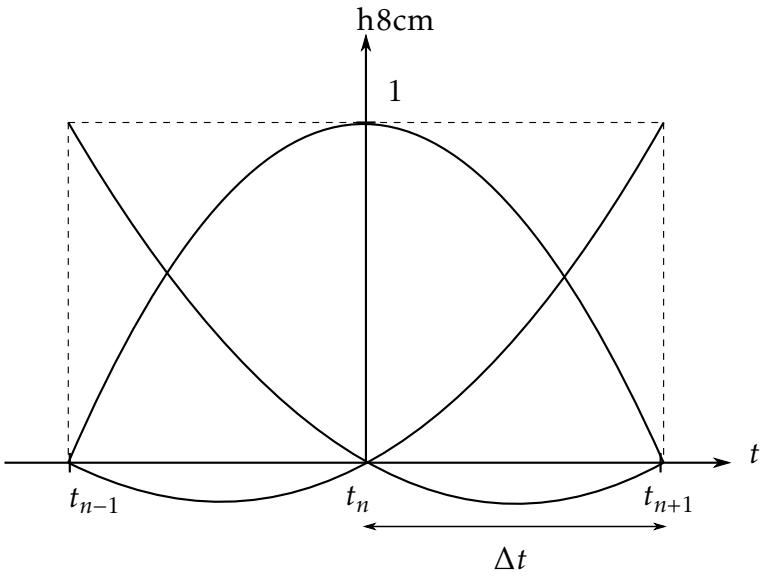

Figure 3.1: Quadratic basis functions

becomes:

$$\begin{pmatrix} a & b & c & 0 & & \cdots & \cdots & & 0 \\ b & d & b & 0 & 0 & & & & \\ c & b & 2a & b & c & 0 & & & \vdots \\ 0 & 0 & b & d & b & 0 & 0 & & \vdots \\ & 0 & c & b & 2a & b & c & \ddots & \\ \vdots & & \ddots & \ddots & \ddots & \ddots & \ddots & \ddots & 0 \\ \vdots & & & 0 & c & b & 2a & b & c \\ & & & & 0 & 0 & b & d & b \\ 0 & & \cdots & \cdots & & 0 & c & b & a \end{pmatrix} \begin{pmatrix} u_1 \\ u_2 \\ \\ \vdots \\ \\ \vdots \\ \\ u_{N+1} \end{pmatrix} = \begin{pmatrix} f_1 + mv_0 \\ \\ \vdots \\ \\ \vdots \\ \\ \vdots \\ \\ F_{N+1} \end{pmatrix} \tag{3.12}$$

Since $u_1 = u_0$, then one can implement algorithm 4, where:

$$\mathbf{p} = \begin{pmatrix} a \\ b \end{pmatrix} \quad , \quad \mathbf{H} = \begin{pmatrix} c & b & 2a \\ 0 & 0 & b \end{pmatrix} \quad \text{and} \quad \mathbf{A} = \begin{pmatrix} b & c \\ d & b \end{pmatrix}$$

3.1.4 Errors analysis

The considered spring-mass system is the same as the one described in 2.2.2 and the time step is constant. The number of degrees-of-freedom is the same for quadratic and linear models. In figure 3.2, the error for the continuous Galerkin scheme is very closed to the one of the central differences scheme due to the similarities between systems (3.9) and (2.10). In the case of a non constant time step, the computation for the Galerkin scheme is much longer than for the Newmark solution strategy.

One would note that a quadratic approximation of the displacement leads to a piecewise constant acceleration. The linear acceleration scheme (LA) uses

Algorithm 4 Continuous Galerkin for quadratic elements

Require: $\mathbf{A}$, $\mathbf{H}$, and $\mathbf{p}$
Require: Initial conditions: $\mathbf{u}_0$, $\mathbf{v}_0$

$u_1 \leftarrow u_0$
$\mathbf{y}_1 \leftarrow u_1 \cdot \mathbf{p}$
$\begin{pmatrix} u_2 \\ u_3 \end{pmatrix} \leftarrow \mathbf{A}^{-1}\left(\begin{pmatrix} f_1 + mv_0 \\ f_2 \end{pmatrix} - \mathbf{y}_1\right)$
for $n = 3$ **to** $N - 2$ **do**
$\mathbf{y}_n \leftarrow \mathbf{H} \cdot \begin{pmatrix} u_{n-2} \\ u_{n-1} \\ u_n \end{pmatrix}$
$\begin{pmatrix} u_{n+1} \\ u_{n+2} \end{pmatrix} \leftarrow \mathbf{A}^{-1}\left(\begin{pmatrix} F_n \\ F_{n+1} \end{pmatrix} - \mathbf{y}_n\right)$
end for

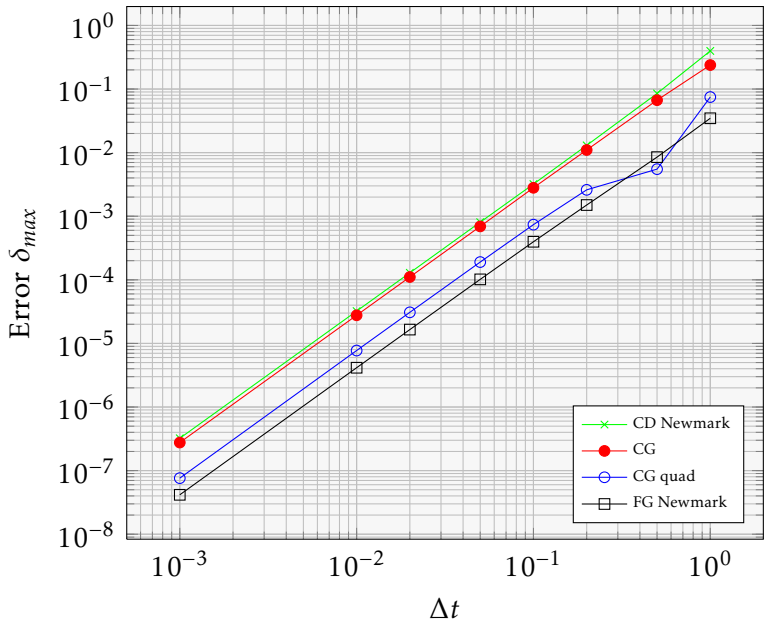

Figure 3.2: Convergence for a continuous Garlerkin scheme

a linear approximation of the acceleration. Nonetheless, while second order accurate, the CGM with quadratic elements is about ten times more accurate than the LA method.

3.2 Space-time finite element method

3.2.1 Formulation

In the previous sections, it was shown for a single degree-of-freedom system continuous Galerkin formulations and Newmar integration schemes share the same properties. Consider the one-dimensional rod described by equation (2.11) for a finite time interval $[0;T]$ where $0 \leq T_c \leq T$. Boundary and initial conditions are now seen as boundary conditions over the space-time

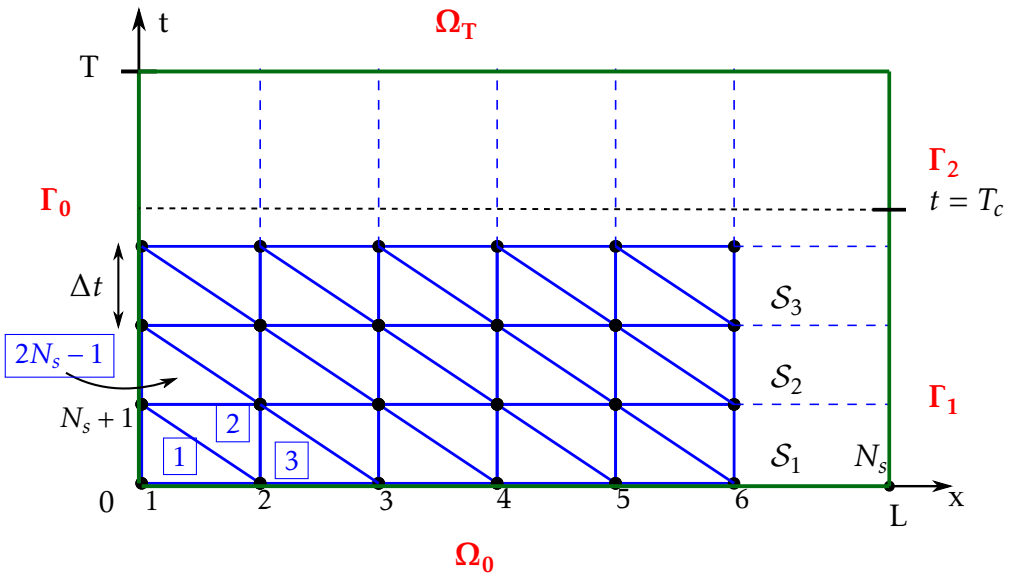

Figure 3.3: Meshed space time domain

domain $\mathcal{S} = \Omega \times \Gamma = [0, L] \times [0, T]$. Using the displacement field as unknown, the following weak formulation is derived:

$$\begin{aligned} &\text{Find } u \in \mathcal{C}_a \\ &\forall \psi \in \mathcal{C}, \quad \int_0^T \int_0^L \left(ES \frac{\partial^2 u}{\partial x^2} - \rho S \frac{\partial^2 u}{\partial t^2} + f_v \right) \psi \, dx \, dt = 0 \end{aligned} \tag{3.13}$$

Through integrations by parts, second-order derivatives in time or space will become first-order derivatives so that linear basis functions are used (cf. remark 3). Since functions are chosen to be continuous over the space-time domain $\mathcal{S}$, integration by part has the following form:

$$\begin{aligned} \int_0^T \int_0^L ES \frac{\partial^2 u}{\partial x^2} \psi \, dx \, dt &= - \int_0^T \int_0^L ES \frac{\partial u}{\partial x} \frac{\partial \psi}{\partial x} \, dx \, dt + \int_0^T ES \left[\frac{\partial u}{\partial x} \psi \right]_0^L dt \\ \int_0^T \int_0^L \rho S \frac{\partial^2 u}{\partial t^2} \psi \, dx \, dt &= - \int_0^T \int_0^L \rho S \frac{\partial u}{\partial t} \frac{\partial \psi}{\partial t} \, dx \, dt + \int_0^L \rho S \left[\frac{\partial u}{\partial t} \psi \right]_0^T dx \end{aligned} \tag{3.14}$$

which leads to the following weak formulation for the rod:

$$\begin{aligned} &\text{Find } u \in \mathcal{C}_a, \ \forall \psi \in \mathcal{C}, \\ &\iint_{\mathcal{S}} \left(ES \frac{\partial u}{\partial x} \frac{\partial \psi}{\partial x} - \rho S \frac{\partial u}{\partial t} \frac{\partial \psi}{\partial t} \right) dx \, dt - \int_0^T S g \psi(L) \, dt = \\ &\qquad \iint_{\mathcal{S}} f_v \psi \, dx \, dt + \int_0^L \rho S v_0 \psi(x, 0) \, dx \end{aligned} \tag{3.15}$$

with

$$\begin{aligned} \mathcal{C}_a &= \{ w \in H^1(\mathcal{S}), \ w = u_0 \text{ on } \Omega_0, \ w = 0 \text{ on } \Gamma_0 \text{ and } w = u_c \text{ on } \Gamma_1 \} \\ \mathcal{C} &= \{ \psi \in H^1(\mathcal{S}), \psi = 0 \text{ on } \Omega_T \text{ and } \psi = 0 \text{ on } \Gamma_0 \} \end{aligned}$$

Remark 3 (Accuracy of the solution)**.** *Since linear functions on $\mathcal{S}$ have been chosen to approximate the displacement, velocity is constant over an finite element and acceleration is zero.*

Due to the space time mesh depicted in figure 3.3, an approximated solution of the form:

$$\forall (x,t) \in \mathcal{S}, \quad u(x,t) = \sum_{i=1}^{N_{\text{dof}}} u_i w_i(x,t) \tag{3.16}$$

is employed. Finite elements are triangles on the 2D space-time map. Mesh is regular in order to facilitate the computation and the time length of a slab Δt is thus constant. It is also worth to notice that remeshing is easier with simplices than with multiplices [1, 18].

Once again $\psi_i(x,t) = w_i(x,t)$ so that one gets symmetric matrices. Since $g = 0$ during the free displacement phase, one can consider the following global vectors and global matrices over the full space time domain for the implementation: $\forall (i,j) \in [\![1, N_{\text{dof}}]\!]^2$,

$$\begin{aligned} \mathbf{M}_{ij} &= \iint_{\mathcal{S}} \rho S \frac{\partial w_j}{\partial t}\frac{\partial \psi_i}{\partial t}\,dx\,dt \quad ; \quad \mathbf{K}_{ij} = \iint_{\mathcal{S}} ES \frac{\partial w_j}{\partial x}\frac{\partial \psi_i}{\partial x}\,dx\,dt \\ \mathbf{f}_i &= \iint_{\mathcal{S}} f_v \psi_i\,dx\,dt \quad ; \quad \lambda_{\mathbf{0}i} = \int_0^L \rho S v_0(x)\psi_i(x,0)\,dx \end{aligned} \tag{3.17}$$

These global matrices and vectors are large and should not be numerically implemented as such. The solution method processes iteratively for each slab instead.

Remark 4 (Line of integration)**.** *In the case of an non laminated and regular mesh as the one illustrated in figure 3.3, slabs are not defined in the same way. One can use a space-time integration line as proposed in [1, p.77].*

Triangle based formulation Considering regular and laminated meshes as well as the numbering of nodes in figure 3.3 and a constant Δt (see remark **??**), elementary matrices are built from triangular elements (3.18) and then assembled for each time slabs $\mathcal{S}_n$. Such that $\forall k \in [\![1, N_e]\!], \forall (i,j,) \in [\![1,3]\!]^2$,

$$\begin{aligned} \mathbf{M_k}_{ij} &= \int_0^{1-x_r}\int_0^1 \rho S\left(\frac{\partial w_{ri}}{\partial x_r}\frac{\partial x_r}{\partial t} + \frac{\partial w_{ri}}{\partial t_r}\frac{\partial t_r}{\partial t}\right)\left(\frac{\partial w_{rj}}{\partial x_r}\frac{\partial x_r}{\partial t} + \frac{\partial w_{rj}}{\partial t_r}\frac{\partial t_r}{\partial t}\right)J_{\phi_k}\,dx_r\,dt_r \\ \mathbf{K_k}_{ij} &= \int_0^{1-x_r}\int_0^1 ES\left(\frac{\partial w_{ri}}{\partial x_r}\frac{\partial x_r}{\partial x} + \frac{\partial w_{ri}}{\partial t_r}\frac{\partial t_r}{\partial x}\right)\left(\frac{\partial w_{rj}}{\partial x_r}\frac{\partial x_r}{\partial x} + \frac{\partial w_{rj}}{\partial t_r}\frac{\partial t_r}{\partial x}\right)J_{\phi_k}\,dx_r\,dt_r \\ &\text{with} \quad w_{r1} = 1 - x_r - t_r,\ w_{r2} = x_r, \text{ and } w_{r3} = t_r \end{aligned} \tag{3.18}$$

where N_e is the number of elements per slab and J_{ϕ_k} is the Jacobian determinant of the transformation from T_r (the triangular reference element) to T_k (the real element):

$$\phi_k : \begin{pmatrix} T_r & \to & T_k \\ (x_r, t_r) & \mapsto & (x,t) \end{pmatrix} \tag{3.19}$$

Quadrangle based formulation Using the same regular and laminated mesh as previously but with rectangular elements, the basis functions (4.28) should be considered and reorganized as: $\forall i \in [\![1,4]\!],\ w_i(x,t) = f_i(x)g_i(t)$. Accordingly, mass and stiffness elementary matrices from (3.17) read:

$$\begin{aligned} \mathbf{M}_{ij} &= \rho S \int_0^L f_i f_j \, dx \int_0^T \frac{\partial g_i}{\partial t}\frac{\partial g_j}{\partial t} \, dt \\ \mathbf{K}_{ij} &= ES \int_0^T g_i g_j \, dt \int_0^L \frac{\partial f_i}{\partial x}\frac{\partial f_j}{\partial x} \, dx \end{aligned} \tag{3.20}$$

and the analytical expressions for the elementary matrices are:

$$\mathbf{K_e} = \frac{\Delta t}{6\Delta x}\begin{pmatrix} 2 & -2 & -1 & 1 \\ -2 & 2 & 1 & -1 \\ -1 & 1 & 1 & -1 \\ 1 & -1 & -1 & 1 \end{pmatrix} \quad ; \quad \mathbf{M_e} = \frac{\Delta x}{6\Delta t}\begin{pmatrix} 2 & 1 & -1 & -2 \\ 1 & 2 & -2 & -1 \\ -1 & -2 & 2 & 1 \\ -1 & -1 & 1 & 2 \end{pmatrix} \tag{3.21}$$

3.2.2 Numerical scheme and implementation

Assembling matrices $\mathbf{M}$ and $\mathbf{K}$ and assuming $f_v = 0$, the following linear system to be solved is obtained:

$$(\mathbf{K} - \mathbf{M})\mathbf{u} = \mathbf{f} + \lambda_0 \quad \Leftrightarrow \quad \mathbf{R}\mathbf{u} = \mathbf{F} \tag{3.22}$$

which is the matrix counterpart of (3.7):

$$\begin{pmatrix} \mathbf{A} & \mathbf{B} & \mathbf{0} & \cdots & \mathbf{0} \\ \mathbf{B}^t & 2\mathbf{A} & \mathbf{B} & & \vdots \\ \mathbf{0} & \ddots & \ddots & \ddots & \mathbf{0} \\ \vdots & & \mathbf{B}^t & 2\mathbf{A} & \mathbf{B} \\ \mathbf{0} & \cdots & \mathbf{0} & \mathbf{B}^t & 2\mathbf{A} \end{pmatrix}\begin{pmatrix} \mathbf{u}_1 \\ \\ \vdots \\ \\ \mathbf{u}_{N+1} \end{pmatrix} = \begin{pmatrix} \mathbf{f}_1 + m\mathbf{v}_0 \\ \\ \vdots \\ \\ \mathbf{F}_{N+1} \end{pmatrix} \tag{3.23}$$

where N_s denotes the number of nodes at the interface between $\mathcal{S}_{n-1}$ and $\mathcal{S}_n$, assumed to be constant, and N denotes the number of time slabs. If $N_D = N \times N_s$ the size of $\mathbf{u}$ and $\mathbf{F}$ is N_D, the size of $\mathbf{R}$ is $N_D \times N_D$, the size of $\mathbf{A}$ and $\mathbf{B}$ is $N_s \times N_s$, and the size $\mathbf{u}_n$ is N_s.

Similarly as in section 3.1.2, the very large matrix $\mathbf{R}$ is replaced smaller matrices $\mathbf{A}$ and $\mathbf{B}$, and an iterative numerical scheme is implemented, which would lead to the following procedure $\forall n \in [\![3,N]\!]$:

$$\forall n \in [\![3,N]\!], \quad \mathbf{B}\mathbf{u}_{n+1} = \mathbf{B}^{-1}(\mathbf{F}_n - \mathbf{B}^t\mathbf{u}_{n-1} - 2\mathbf{A}\mathbf{u}_n) \tag{3.24}$$

For each time step $n \in [\![1,N]\!]$, the first and the last components of $\mathbf{u}_n$ are known ($\mathbf{u}_{n1} = 0$ and $\mathbf{u}_{nN_s} = \mathbf{u}_n^2 = u_c$, see equation (2.15)). Accordingly, matrices $\mathbf{A}$ and $\mathbf{B}$ can be reduced to size $(N_s - 1) \times (N_s - 1)$, by discarding the first row and the first column corresponding to the clamped DoF. Then, the method exposed in 2.3.2 can be used with matrices (3.25) where $\mathbf{B}_{22}$, $\mathbf{A}_{22}$ and $\mathbf{u}_\mathbf{n}^2$ are scalars.

$$\mathbf{B} = \begin{bmatrix} \mathbf{B}_{11} & \mathbf{B}_{12} \\ \mathbf{B}_{21} & \mathbf{B}_{22} \end{bmatrix}, \quad \mathbf{A} = \begin{bmatrix} \mathbf{A}_{11} & \mathbf{A}_{12} \\ \mathbf{A}_{21} & \mathbf{A}_{22} \end{bmatrix} \tag{3.25}$$

and

$$\forall n \in [\![3, N]\!], \quad \mathbf{u}_n = \begin{pmatrix} \mathbf{u}_n^1 \\ \mathbf{u}_n^2 \end{pmatrix}, \quad \mathbf{F}_n = \begin{pmatrix} \mathbf{F}_n^1 \\ \mathbf{F}_n^2 \end{pmatrix} \tag{3.26}$$

Therefore, algorithm 5 can be implemented.

Algorithm 5 CG time integration scheme for enforced/free displacement

Require: $\mathbf{A}$, $\mathbf{B}$, u_c
Require: Initial conditions: $\mathbf{u}_0$, $\mathbf{v}_0$
$\mathbf{u}_1 \leftarrow \mathbf{u}_0$
$\mathbf{u}_2^1 \leftarrow \mathbf{B}_{11}^{-1}(\mathbf{F}_1^1 - \mathbf{A}_{11}\mathbf{u}_1^1 - \mathbf{A}_{12}\mathbf{u}_1^2 - \mathbf{B}_{12}\mathbf{u}_2^2)$
$\mathbf{u}_2^2 \leftarrow u_c(t_2)$
Enforced displacement phase:
for $n = 3$ **to** N_{T_c} **do**
  $\mathbf{u}_n^2 \leftarrow u_c(t_n)$
  $\mathbf{u}_n^1 \leftarrow \mathbf{B}_{11}^{-1}(\mathbf{F}_{n-1}^1 - 2\mathbf{A}_{11}\mathbf{u}_{n-1}^1 - 2\mathbf{A}_{12}\mathbf{u}_{n-1}^2 - \mathbf{B}_{12}\mathbf{u}_n^2 - \mathbf{B}_{11}^t\mathbf{u}_{n-2}^1 - \mathbf{B}_{12}^t\mathbf{u}_{n-2}^2)$
end for
Transition:
$\mathbf{u}_{N_{T_c}} \leftarrow (\mathbf{u}_{N_{T_c}}^1; \mathbf{u}_{N_{T_c}}^2)$
Free displacement phase:
for $n = N_{T_c}$ **to** N **do**
  $\mathbf{u}_n \leftarrow \mathbf{B}^{-1}(\mathbf{F}_{n-1} - 2\mathbf{A}\mathbf{u}_{n-1} - \mathbf{B}^t\mathbf{u}_{n-2})$
end for

3.2.3 Results

The investigated rod has the mechanical properties defined in section 2.3.3 with $f_v = 0$ and $v_0 = 0$. Are compared in figure 3.4 and 3.5 the central difference Newmark scheme with lumped and consistent mass, respectively, to continuous Galerkin scheme with triangular or rectangular elements. It is worthy to note that Garlerkin and central difference scheme are equivalent when the lumped mass option is selected. Also the results given by the Newmark scheme with consistent mass are identical to those of a continuous Galerkin scheme with rectangular elements. Convergence properties look identical for a continuous Galerkin approach with triangular or rectangular elements and central difference technique with a lumped mass. Also, Newmark schemes with lumped mass (see 2.1.3) and Galerkin scheme converge only if $c\Delta t < \Delta x$ (CFL condition).

Figure 3.5 shows that with rectangular elements, information progates in the rod with unbounded velocity. This yields spurious oscillations *before* the prescribed displacement command. This phenomena is not observable when triangular elements are chosen. Displacement at a point of a rod is rigorously zero before the initial travelling wave reaches this point.

High-frequency oscillations keep existing as opposed to the theoretical solution. These oscillations only depend on the mesh size in space Δx. The number of oscillations increases and their amplitude decreases with Δx as illustrated in figure 3.6.

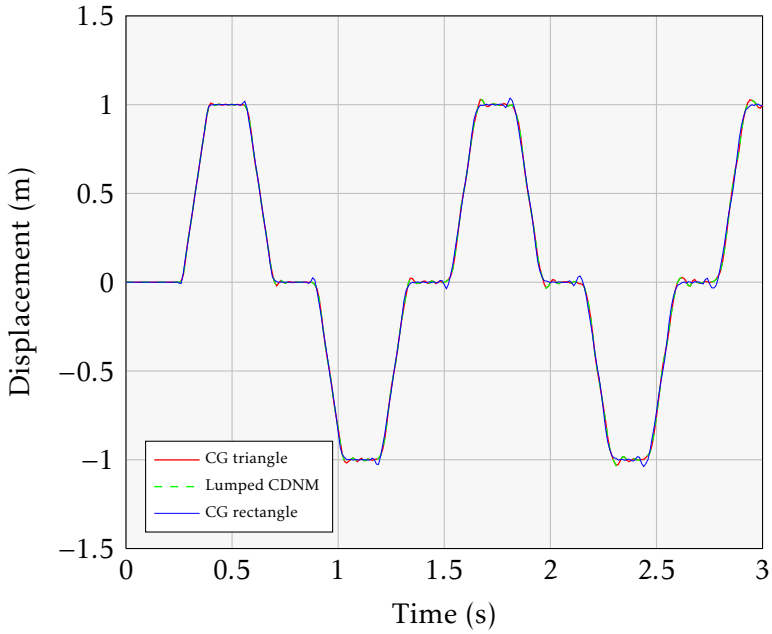

Figure 3.4: Response at $x = \frac{L}{2}$ to a ramp entry for $\Delta t = 10^{-2}$ s and $\Delta x = \frac{L}{30}$

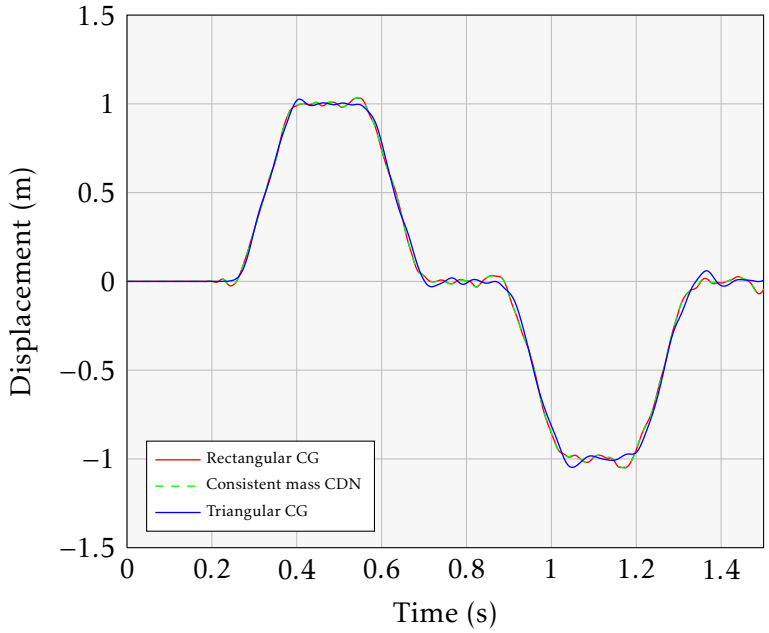

Figure 3.5: Response at $x = L/2$ to a ramp entry for $\Delta t = 10^{-3}$ s and $\Delta x = L/30$

Finally, when linear functions in time are used, a continuous Galerkin scheme with triangular elements is equivalent to a central differences Newmark scheme with lumped mass. A continuous Galerkin scheme with rectangular elements is equivalent to a central differences Newmark scheme with consistent mass matrix.

Ramp with an infinite slope A discontinuity due to the displacement window has been introduced. All spurious phenomena described before are ampli-

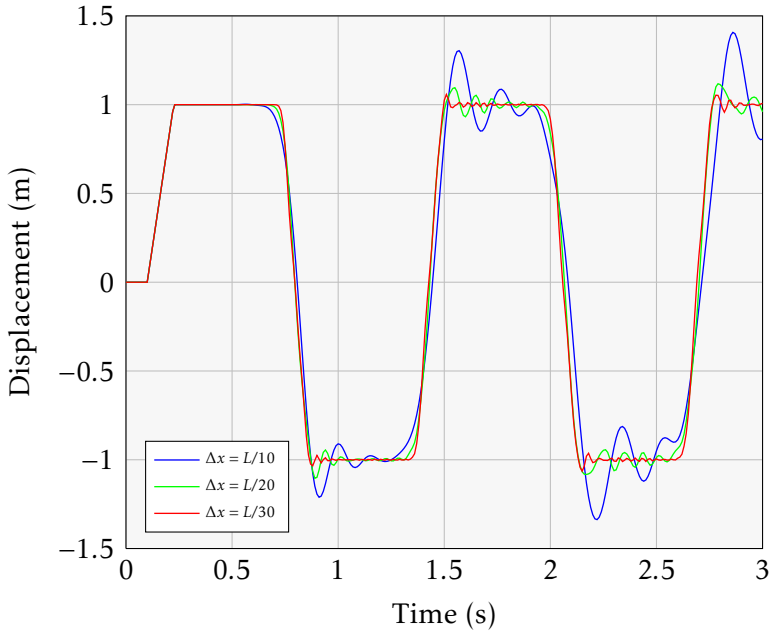

Figure 3.6: Convergence of CG methods for a ramp entry at $x = L$ for $\Delta t = 10^{-2}$ s

fied. This discontinuity is shown in figure 3.7: the prescribed displacement at the end of the rod causes much larger amplitude spurious high-frequency oscillations than with finite slope displacement command, even when triangular elements are used.

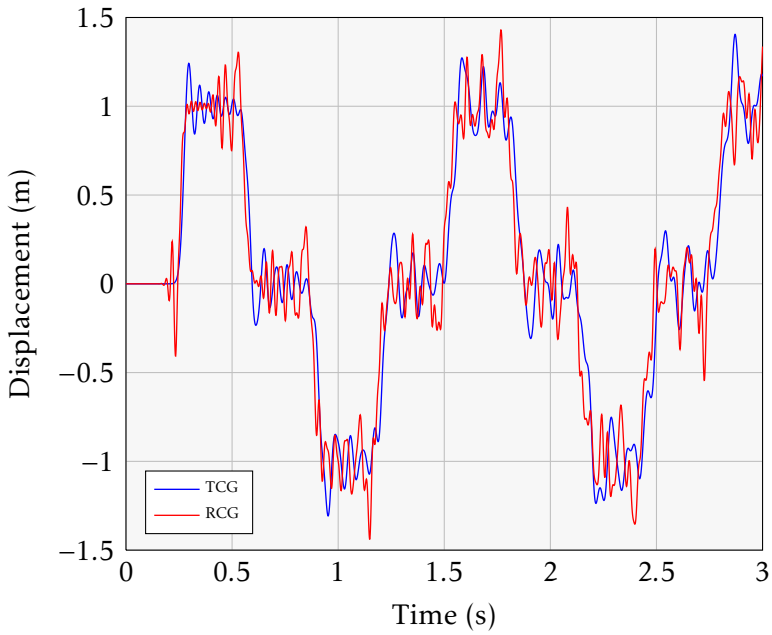

Figure 3.7: Response at $x = L/2$ to a ramp entry with an infinite slope for $\Delta t = 10^{-3}$ s and $\Delta x = L/30$

Chapter 4

Discontinuous Galerkin Methods

In previous chapters, it was shown that time integration schemes may generate spurious high-frequency oscillations in the response when the external loading tends to be nonsmooth. In order to mitigate these undesirable phenomena, discontinuous Galerkin methods were introduced for elastodynamics [11, 14]. The main idea of this class of tehcniques is to assume space-time discontinuous basis functions in the discretization. The method was first introduced in fluid mechanic to capture sharp gradients in the solution. It was implemented with a h-adaptivity[1] [26] and the stability and the convergence of the method is analysed in [10, 17]. In [13], Hulbert compares single-field and two-field formulations for discontinuous Galerkin methods: both formulations are stable and convergent.

4.1 Derivation in time domain

The method is introduced in the time domain only.

4.1.1 Formulation

Equation (3.1) is written within a two-field formulation, diplacement and velocity:

$$m\dot{v}(t) + ku(t) = f(t) \tag{4.1}$$
$$v(t) - \dot{u}(t) = 0 \tag{4.2}$$
$$u(0) = u_0 \quad v(0) = v_0 \tag{4.3}$$

As illustrated in figure 4.1, the discontinuous Galerkin method is characterized by the presence of discontinuities in the solution at different intants t_n. This greatly helpds capturing potential sharp gradients. In other words, the continuity of the unknown fields is weakly enforced at time t_n:

$$[u(t)] = u(t^+) - u(t^-) = 0 \tag{4.4}$$
$$[v(t)] = v(t^+) - v(t^-) = 0 \tag{4.5}$$

[1] hp-FEM are FEM using mesh size h and polynomial degree p as elements of variables.

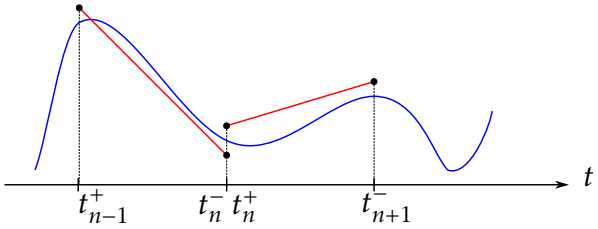

Figure 4.1: Discontinuous linear approximation

This conditions may be enforced through penalties [3] which yields the following weak two-field formulation:

$$\text{Find } (u,v) \in \mathcal{C}_u \times \mathcal{C}_v, \quad \forall (\psi_1,\psi_2) \in \mathcal{C}_1 \times \mathcal{C}_2, \tag{4.6}$$

$$\int_0^T (ku + m\dot{v} - f)\psi_1 dt + \sum_n c_1[v(t_n)]\psi_1(t_n) = 0 \tag{4.7}$$

$$\int_0^T (c_3(\dot{u} - v))\psi_2 dt + \sum_n c_2[u(t_n)]\psi_2(t_n) = 0 \tag{4.8}$$

where c_1, c_2 and c_3 are constants to be chosen. In this formulation, piecewise linear functions are going to be employed for the approximation of u and v. Since the same approximation basis is chosen for u and v, $\mathcal{C}_u = \mathcal{C}_v = \mathcal{C}_1 = \mathcal{C}_2 = C_p^0([0,T])$. By discretizing the time domain $[0,T]$ as pictured in figure 4.1 and looking for u and v under the form: $\forall t \in [0;T]$,

$$u(t) = \sum_{i=0}^{N} u_i^+ w_{1i}(t) + u_i^- w_{2i}(t) \tag{4.9}$$

$$v(t) = \sum_{i=0}^{N} v_i^+ w_{1i}(t) + v_i^- w_{2i}(t) \tag{4.10}$$

one obtain the following discrete two-field weak formulation:

$$\text{Find } (u,v) \in \mathcal{C}_u \times \mathcal{C}_v, \quad \forall (\psi_1,\psi_2) \in \mathcal{C}_1 \times \mathcal{C}_2, \tag{4.11}$$

$$\sum_{n=0}^{N} \left(\int_{t_n^+}^{t_{n+1}^-} (ku + m\dot{v})\psi_1 dt + c_1[v(t_n)]\psi_1(t_n) \right) = \sum_{n=0}^{N} \int_{t_n^+}^{t_{n+1}^-} f\psi_1 dt \tag{4.12}$$

$$\sum_{n=0}^{N} \left(\int_{t_n^+}^{t_{n+1}^-} c_3(\dot{u} - v)\psi_2 dt + c_2[u(t_n)]\psi_2(t_n) \right) = 0 \tag{4.13}$$

Remark 5 (Numerical fluxes)**.** *The continuity enforcement through penalties is a way to connect elements to each other. Indeed since discontinuities are allowed between elements, each element is initially independent. Another way to connect elements together is to enforce numerical fluxes between elements. This method is mainly used for convection-diffusion problems in fluid dynamics [20] but can be adapted to elastodynamics. Nonetheless the choice of the numerical flux is not obvious [5] since it may affect the stabitlity and the accuracy of the DGFEM [3].*

4.1.2 Numerical scheme and implementation

Considering the following unknown vector :

$$\mathbf{q}_n^t = \begin{pmatrix} u_n^+ & u_{n+1}^- & v_n^+ & v_{n+1}^- \end{pmatrix} \tag{4.14}$$

the system to be solved for each time step t_n is :

$$\forall n \in [0, N], \quad \mathbf{A}_n \mathbf{q}_n = \mathbf{f}_n \tag{4.15}$$

where $\mathbf{A}_n = \mathbf{A}'_n + \mathbf{A}''_n$ with

$$\mathbf{A}'_n = \int_{t_n^+}^{t_{n+1}^-} \begin{pmatrix} kw_{1n}\psi_{1n} & kw_{2n}\psi_{1n} & m\dot{w}_{1n}\psi_{1n} & m\dot{w}_{1n}\psi_{1n} \\ kw_{1n}\psi_{2n} & kw_{2n}\psi_{2n} & m\dot{w}_{1n}\psi_{2n} & m\dot{w}_{2n}\psi_{2n} \\ c_3\dot{w}_{1n}\psi_{1n} & c_3\dot{w}_{1n}\psi_{1n} & -c_3 w_{1n}\psi_{1n} & -c_3 w_{2n}\psi_{1n} \\ c_3\dot{w}_{1n}\psi_{2n} & c_3\dot{w}_{2n}\psi_{2n} & -c_3 w_{1n}\psi_{2n} & -c_3 w_{2n}\psi_{2n} \end{pmatrix} dt \tag{4.16}$$

and

$$\mathbf{A}''_n = \begin{pmatrix} 0 & 0 & c_1\psi_{1n}(t_n) & 0 \\ 0 & 0 & 0 & 0 \\ 0 & c_2\psi_{1n}(t_n) & 0 & 0 \\ 0 & 0 & 0 & 0 \end{pmatrix} \tag{4.17}$$

The external forcing is expressed as follows:

$$\mathbf{f}_n = \begin{pmatrix} \int_{t_n^+}^{t_{n+1}^-} f\psi_{1n} dt + c_1 v(t_n^-) \\ \int_{t_n^+}^{t_{n+1}^-} f\psi_{2n} dt \\ c_2 u(t_n^-) \\ 0 \end{pmatrix} \tag{4.18}$$

Matrix $\mathbf{A}_n$ has interesting numerical properties for the following three penalty paramters: $c_1 = m$, $c_2 = k$ and $c_3 = k$ [3, 26]. Linear time dicontinuous trial functions are assumed so that $\psi_{1i} = w_{1i}$ and $\psi_{2i} = w_{2i}$. Also, any external body force is neglected, i.e. $f = 0$. Accordingly, expression (4.15) becomes:

$$\begin{pmatrix} \frac{1}{3}\Delta tk & \frac{1}{6}\Delta tk & -\frac{1}{2}m + c_1 & \frac{1}{2}m \\ \frac{1}{6}\Delta tk & \frac{1}{3}\Delta tk & -\frac{1}{2}m & \frac{1}{2}m \\ -\frac{1}{2}c_3 + c_2 & \frac{1}{2}c_3 & -\frac{1}{3}\Delta t c_3 & -\frac{1}{6}\Delta t c_3 \\ -\frac{1}{2}c_3 & \frac{1}{2}c_3 & -\frac{1}{6}\Delta t c_3 & -\frac{1}{3}\Delta t c_3 \end{pmatrix} \begin{pmatrix} u_n^+ \\ u_{n+1}^- \\ v_n^+ \\ v_{n+1}^- \end{pmatrix} = \begin{pmatrix} c_1 v(t_n^-) \\ 0 \\ c_2 u(t_n^-) \\ 0 \end{pmatrix} \tag{4.19}$$

For a constant time step Δt, matrix $\mathbf{A}_n$ is also constant and named $\mathbf{A}$. Then the time integration scheme is quite simple as described by algorithm 6.

4.1.3 Errors analysis

Spring-mass system described in section 3.1.4 is used. The DGFEM implies two values at each time step t_n and the global error is estimated at times t_n^+.

Algorithm 6 Discontinuous Galerkin time integration scheme

Require: c_1, c_2 and $\mathbf{A}$, Initial conditions: u_0, v_0
  $u_0^- \leftarrow u_0$
  $v_0^- \leftarrow v_0$
  for $n = 0$ **to** N **do**
    $u(t_n^-) \leftarrow u_n^-$
    $v(t_n^-) \leftarrow v_n^-$
    $\begin{pmatrix} u_n^+ & u_{n+1}^- & v_n^+ & v_{n+1}^- \end{pmatrix}^T \leftarrow \mathbf{A}^{-1} \begin{pmatrix} c_1 v(t_n^-) & 0 & c_2 u(t_n^-) & 0 \end{pmatrix}^T$
  end for

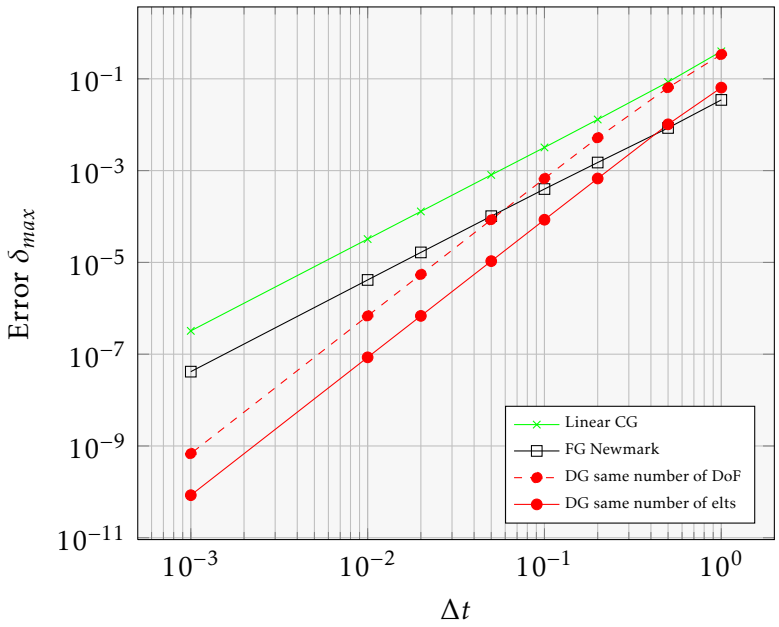

Figure 4.2: Convergence rate for discontinuous Garlerkin scheme

In figure 4.2, DGFEM error is compared to Newmark schemes. One can see that a DG scheme is much more accurate and converge faster than all schemes described and use so far. For $\Delta t = 10^{-3}$, DGFEM is 100 to 1000 times more accurate than the Fox-Goodwin scheme which is 10 times more accurate than CGFEM. However one should note that DGM uses two values for each approximated field at each time step. Therefore, for the same number of elements, the number of DoF is twice larger than for a linear Newmark method or a linear CGM (if N_e is the number of elements, in the linear case $N = N_e + 1$ for Newmark or CG while $N = 2N_e$ for DG). One can see that DG method is third order accurate, ie, $\delta_{\max} \sim \Delta t^3$ when $\Delta t \to 0$. Even with twice less elements, the dicontinuous Galerkin method is still more accurate than other methods.

4.2 Space-time discontinuous finite element method

4.2.1 Formulation

The same way as the 1DoF system, a two-field formulation is now derived. Consider equations (2.11) for a finite time interval $[0;T]$ to which the velocity definition is added : $\forall (x,t) \in [0;L]\times]0;T[$,

$$\begin{aligned} &ES\frac{\partial^2 u}{\partial x^2}(x,t) + f_v = \rho S\frac{\partial v}{\partial t}(x,t) \\ &\frac{\partial u}{\partial t}(x,t) = v(x,t) \end{aligned} \tag{4.20}$$

with boundary conditions ($0 \leq T_c \leq T$) :

$$\begin{aligned} &\forall t \in [0;T[, \quad u(0,t) = 0 \\ &\forall t \in [0;T_c[, \quad u(L,t) = u_c(t) \\ &\forall t \in [T_c;T[, \quad E\frac{\partial u}{\partial x}(L,t) = g(t) \end{aligned} \tag{4.21}$$

and initial conditions :

$$\begin{aligned} &\forall x \in [0,L], \quad u(x,0) = u_0(x) \\ &\forall x \in [0,L], \quad \frac{\partial u}{\partial t}(x,0) = v_0(x) \end{aligned} \tag{4.22}$$

Similarly to what was done in section 4.1.1, displacement continuity has to be enforced at each time t. Integration over slabs $\mathcal{S}_n = \Omega \times [t_{n-1}^+ ; t_n^-]$ for $n \in [1,N]$, domain displayed in figure 4.3, is considered. With both displacement and velocity as unknown fields, two trial functions ψ_1 and ψ_2 are required. Then, the following weak formulation is derived:

$$\begin{aligned} &\text{Find } (u,v) \in \mathcal{C}_u \times \mathcal{C}_v, \quad \forall (\psi_1,\psi_2) \in \mathcal{C}_1 \times \mathcal{C}_2, \quad \forall n \in [1,N], \\ &\iint_{\mathcal{S}_n} \Big(ES\frac{\partial^2 u}{\partial x^2}(x,t) - \rho S\frac{\partial v}{\partial t}(x,t)) + f_v\Big)\psi_1 dxdt \\ &\qquad\qquad + \int_\Omega C_1[v(x,t_{n-1})]\psi_1(x,t_{n-1}^+)dx = 0 \\ &\iint_{\mathcal{S}_n} C_3\Big(\frac{\partial u}{\partial t}(x,t) - v(x,t)\Big)\psi_2 dxdt + \int_\Omega C_2[u(x,t_{n-1})]\psi_2(x,t_{n-1}^+)dx = 0 \end{aligned} \tag{4.23}$$

Integration by part of the term with second order derivatives in space yields

$$\iint_{\mathcal{S}_n} ES\frac{\partial^2 u}{\partial x^2}\psi_1 dxdt = -\iint_{\mathcal{S}_n} ES\frac{\partial u}{\partial x}\frac{\partial \psi_1}{\partial x}dxdt + \int_{t_{n-1}^+}^{t_n^-} ES\Big[\frac{\partial u}{\partial x}\psi_1\Big]_0^L dt \tag{4.24}$$

Accordingly, the following weak two-field formulation is obtained for the system of equations (4.20), (4.21) and (4.22):

$$\begin{aligned}
&\text{Find } (u,v)\in\mathcal{C}_u\times\mathcal{C}_v,\quad \forall(\psi_1,\psi_2)\in\mathcal{C}_1\times\mathcal{C}_2,\quad \forall n\in[1,N],\\
&\iint_{\mathcal{S}_n} ES\frac{\partial u}{\partial x}(x,t)\frac{\partial \psi_1}{\partial x}dxdt+\iint_{\mathcal{S}_n}\rho S\frac{\partial v}{\partial t}(x,t)\psi_1 dxdt-\int_{t_{n-1}^+}^{t_n^-} Sg\psi_1(L,t)dt\\
&\qquad\qquad+\int_\Omega C_1[v(x,t_{n-1})]\psi_1(x,t_{n-1}^+)dx=\iint_{\mathcal{S}_n} f_v\psi_1 dxdt\\
&\iint_{\mathcal{S}_n} C_3\Big(\frac{\partial u}{\partial t}(x,t)-v(x,t)\Big)\psi_2 dxdt+\int_\Omega C_2[u(x,t_{n-1})]\psi_2(x,t_{n-1}^+)dx=0
\end{aligned}\tag{4.25}$$

within the following functional spaces :

$$\begin{aligned}
\mathcal{C}_u&=\{w\in H_p^1(\mathcal{S}),\ w=u_0 \text{ on } \Omega_0,\ w=0 \text{ on } \Gamma_0 \text{ and } w=u_c \text{ on } \Gamma_1\}\\
\mathcal{C}_v&=\{w\in H_p^1(\mathcal{S}),\ w=v_0 \text{ on } \Omega_0,\ w=0 \text{ on } \Gamma_0 \text{ and } w=\dot{u}_c \text{ on } \Gamma_1\}\\
\mathcal{C}_1&=\{\psi\in H_p^1(\mathcal{S}),\psi=0 \text{ on } \Gamma_0\}\\
\mathcal{C}_2&=H_p^1(\mathcal{S})
\end{aligned}$$

For the sake of simplicity, $g=0$, $f_v=0$, $u_0=0$ and $v_0=0$. Also, the same approximation has been chosen for u and v such that $\psi_1=\psi_2$ and $\mathcal{C}_2=\mathcal{C}_1=\{\psi\in H_p^1(\mathcal{S}),\psi=0 \text{ on } \Gamma_0\}$. The solution is sought in the form:

$$\forall(x,t)\in\mathcal{S}_n,\quad u(x,t)=\sum_{i=1}^{N_d}u_i w_i(x,t)\quad\text{and}\quad v(x,t)=\sum_{i=1}^{N_d}v_i w_i(x,t)\tag{4.26}$$

where N_d is the number of DoF per slab and $\psi_i=w_i$.

Several formulations are possible depending on the type of elements chosen for the FEM. $\forall(i,j,n)\in[\![1,N_d]\!]^2\times[\![1,N]\!]$,

$$\begin{aligned}
\mathbf{M_u}_{ijn}&=\iint_{\mathcal{S}_n}\rho S\frac{\partial w_j}{\partial t}\psi_i dxdt\quad;\quad \mathbf{M_v}_{ijn}=\iint_{\mathcal{S}_n}C_3\frac{\partial w_j}{\partial t}\psi_i dxdt\\
\mathbf{K_u}_{ijn}&=\iint_{\mathcal{S}_n}ES\frac{\partial w_j}{\partial x}\frac{\partial \psi_i}{\partial x}dxdt\quad;\quad \mathbf{Q}_{ijn}=\iint_{\mathcal{S}_n}C_3 w_j\psi_i dxdt\\
\mathbf{\Lambda_v}_{ijn}&=\int_\Omega C_1 w_j(x,t_{n-1}^+)\psi_i(x,t_{n-1})dx\\
\mathbf{\Lambda_u}_{ijn}&=\int_\Omega C_1 w_j(x,t_{n-1}^+)\psi_i(x,t_{n-1})dx\\
\lambda_{\mathbf{v}in}&=\sum_{j=1}^{N_d}\int_\Omega C_1 u_j w_j(x,t_{n-1}^-)\psi_i(x,t_{n-1})dx\\
\lambda_{\mathbf{u}in}&=\sum_{j=1}^{N_d}\int_\Omega C_2 v_j w_j(x,t_{n-1}^-)\psi_i(x,t_{n-1})dx
\end{aligned}\tag{4.27}$$

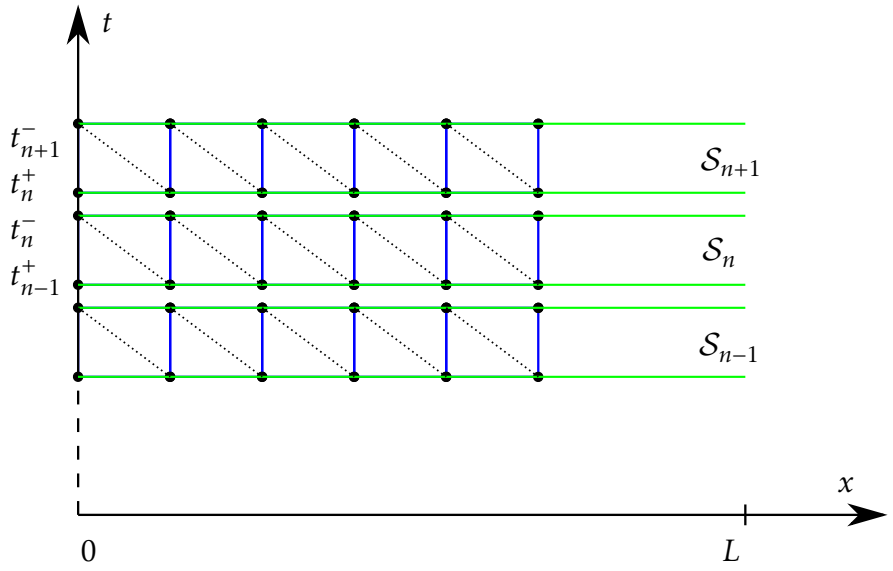

Figure 4.3: Slabs over the space-time discontinuous domain

Quadrangle based formulation In that formulation rectangular elements are chosen with the four basis functions: $\forall(\xi,\zeta)\in[-1\,;1]^2$,

$$\begin{aligned}\hat{w}_1(\xi,\zeta)&=\frac{1}{4}(1-\xi)(1-\zeta)\quad;\quad \hat{w}_2(\xi,\zeta)=\frac{1}{4}(1+\xi)(1-\zeta)\\ \hat{w}_3(\xi,\zeta)&=\frac{1}{4}(1+\xi)(1+\zeta)\quad;\quad \hat{w}_2(\xi,\zeta)=\frac{1}{4}(1+\xi)(1+\zeta)\end{aligned}\tag{4.28}$$

Time and space are uncoupled in the expression of the basis functions (4.28) and one can write:

$$w_i(x,t)=f_i(x)g_i(t)\tag{4.29}$$

and accordingly $\forall(i,j,n)\in[\![1,N_d]\!]^2\times[\![1,N]\!]$,

$$\begin{aligned}\iint_{\mathcal{S}_n}\frac{\partial w_j}{\partial t}w_i\,dxdt&=\int_0^L f_if_j\,dx\int_{t_{n-1}^+}^{t_n^-}\frac{\partial g_j}{\partial t}g_i\,dt\\ \iint_{\mathcal{S}_n}\frac{\partial w_j}{\partial x}\frac{\partial w_i}{\partial x}\,dxdt&=\int_{t_{n-1}^+}^{t_n^-}g_ig_j\,dt\int_0^L\frac{\partial f_j}{\partial x}\frac{\partial f_i}{\partial x}\,dx\\ \iint_{\mathcal{S}_n}w_jw_i\,dxdt&=\int_0^L f_if_j\,dx\int_{t_{n-1}^+}^{t_n^-}g_ig_j\,dt\\ \int_\Omega w_jw_i\,dx&=g_ig_j\int_\Omega f_jf_i\,dx\end{aligned}\tag{4.30}$$

The number of spatial nodes at time t_n^+ is $N_s=N_d/2$. Mass matrix $\mathbf{M}$ and stiffness matrix $\mathbf{K}$ are defined $\forall(i,j)\in[\![1,N_s]\!]^2$ as :

$$\mathbf{M}_{ij}=\int_0^L\rho S f_if_j\,dx\quad;\quad\mathbf{K}_{ij}=\int_0^L ES\frac{\partial f_i}{\partial x}\frac{\partial f_j}{\partial x}\,dx\tag{4.31}$$

Choosing $C_1 = C_2 = C_3 = \rho S$, the matricial system (4.32) is derived. It is the same system as (4.19), in the case where $c_1 = c_2 = c_3 = m$, generalized to higher dimension.

$$\begin{pmatrix} \frac{1}{3}\Delta t\mathbf{K} & \frac{1}{6}\Delta t\mathbf{K} & \frac{1}{2}\mathbf{M} & \frac{1}{2}\mathbf{M} \\ \frac{1}{6}\Delta t\mathbf{K} & \frac{1}{3}\Delta t\mathbf{K} & -\frac{1}{2}\mathbf{M} & \frac{1}{2}\mathbf{M} \\ \frac{1}{2}\mathbf{M} & \frac{1}{2}\mathbf{M} & -\frac{1}{3}\Delta t\mathbf{M} & -\frac{1}{6}\Delta t\mathbf{M} \\ -\frac{1}{2}\mathbf{M} & \frac{1}{2}\mathbf{M} & -\frac{1}{6}\Delta t\mathbf{M} & -\frac{1}{3}\Delta t\mathbf{M} \end{pmatrix} \begin{pmatrix} \mathbf{u}_n^+ \\ \mathbf{u}_{n+1}^- \\ \mathbf{v}_n^+ \\ \mathbf{v}_{n+1}^- \end{pmatrix} = \begin{pmatrix} \mathbf{M}\mathbf{v}_n^- \\ 0 \\ \mathbf{M}\mathbf{u}_n^- \\ 0 \end{pmatrix} \tag{4.32}$$

In [26], Wiberg and Li define the velocity as follows :

$$\forall (x,t) \in [0,L]\times]0;T[, \quad \frac{\partial}{\partial x}\left(\frac{\partial u}{\partial t}(x,t) - v(x,t)\right) = 0 \tag{4.33}$$

which leads to a weak formulation as follows:

$$\begin{aligned} &\text{Find } (u,v) \in \mathcal{C}_u \times \mathcal{C}_v, \quad \forall (\psi_1,\psi_2) \in \times \mathcal{C}_2, \quad \forall n \in [1,N], \\ &\iint_{\mathcal{S}_n} ES\frac{\partial u}{\partial x}(x,t)\frac{\partial \psi_1}{\partial x}dxdt + \iint_{\mathcal{S}_n} \rho S\frac{\partial v}{\partial t}(x,t)\psi_1 dxdt \\ &\qquad + \int_\Omega \rho S[v(x,t_{n-1})]\psi_1(x,t_{n-1}^+)dx = 0 \\ &\iint_{\mathcal{S}_n} ES\frac{\partial}{\partial x}\left(\frac{\partial u}{\partial t}(x,t) - v(x,t)\right)\frac{\partial \psi_2}{\partial x}dxdt + \int_\Omega ES[u(x,t_{n-1})]\psi_2(x,t_{n-1}^+)dx = 0 \end{aligned} \tag{4.34}$$

together with the respective system (4.35) assuming the same approximation as previously:

$$\begin{pmatrix} \frac{1}{3}\Delta t\mathbf{K} & \frac{1}{6}\Delta t\mathbf{K} & \frac{1}{2}\mathbf{M} & \frac{1}{2}\mathbf{M} \\ \frac{1}{6}\Delta t\mathbf{K} & \frac{1}{3}\Delta t\mathbf{K} & -\frac{1}{2}\mathbf{M} & \frac{1}{2}\mathbf{M} \\ \frac{1}{2}\mathbf{K} & \frac{1}{2}\mathbf{K} & -\frac{1}{3}\Delta t\mathbf{K} & -\frac{1}{6}\Delta t\mathbf{K} \\ -\frac{1}{2}\mathbf{K} & \frac{1}{2}\mathbf{K} & -\frac{1}{6}\Delta t\mathbf{K} & -\frac{1}{3}\Delta t\mathbf{K} \end{pmatrix} \begin{pmatrix} \mathbf{u}_n^+ \\ \mathbf{u}_{n+1}^- \\ \mathbf{v}_n^+ \\ \mathbf{v}_{n+1}^- \end{pmatrix} = \begin{pmatrix} \mathbf{M}\mathbf{v}_n^- \\ 0 \\ \mathbf{K}\mathbf{u}_n^- \\ 0 \end{pmatrix} \tag{4.35}$$

The two definitions of the velocity field yield identical results. Nevertheless the classical definition is considered because it is suitable for both quadrangle and triangle based formulations.

Triangle based formulation For triangles, velocity as defined in (4.33) would not be appropriate since polynomial basis functions would linearly couple time and space such that:

$$\forall i \in [\![1,N_d]\!], \quad \frac{\partial^2 w_i}{\partial x \partial t} = 0 \tag{4.36}$$

Formulation (4.25) is thus preferred.

4.2.2 Numerical scheme and implementation

In order to simplify the implementation, a regular laminated mesh with constant time step Δt is assumed. At each time step n, the following linear system should be solved:

$$\begin{bmatrix} \mathbf{K_u} & \mathbf{M_u} + \mathbf{\Lambda_v} \\ \mathbf{M_v} + \mathbf{\Lambda_u} & -\mathbf{Q} \end{bmatrix} \begin{pmatrix} \mathbf{u}_n \\ \mathbf{v}_n \end{pmatrix} = \begin{pmatrix} \lambda_{\mathbf{v}n} \\ \lambda_{\mathbf{u}n} \end{pmatrix} \quad \Leftrightarrow \quad \mathbf{R}\mathbf{q}_n = \mathbf{I}_n \tag{4.37}$$

where matrix $\mathbf{R}$ is constant adn vector $\mathbf{q}$ is of size $4N_p$:

$$\mathbf{q}^t = \left(u_0 \dots u_{N_p}, u_{N_p+1} \dots u_{2N_p}, v_0 \dots v_{N_p}, v_{N_p+1} \dots v_{2N_p}\right) \tag{4.38}$$

Similarly, the clamped DoF should be removed from (4.37) that is to say indexes (for $\mathbf{q}$ and λ) and rows and columns (for $\mathbf{R}$) number 1, N_p+1, $2N_p+2$ and $3N_p+3$. For the phase where displacement is enforced, one refers to 3.2.2: $\forall n \in [\![1, N_{T_c}]\!]$,

$$\begin{bmatrix} \mathbf{R}^*_{11} & \mathbf{R}^*_{12} \\ \mathbf{R}^*_{21} & \mathbf{R}^*_{22} \end{bmatrix} \begin{pmatrix} \mathbf{q}^1_n \\ \mathbf{q}^2_n \end{pmatrix} = \begin{pmatrix} \mathbf{l}^1_n \\ \mathbf{l}^2_n \end{pmatrix} \tag{4.39}$$

where $\mathbf{q}^1_n$ corresponds to the constrained displacement and velocity :

$$\mathbf{q}^1_n = \begin{pmatrix} u_c(t^+_{n-1}) & u_c(t^-_n) & v_c(t^+_{n-1}) & v_c(t^-_n) \end{pmatrix}^t \tag{4.40}$$

and

$$\mathbf{q}^2_n = {\mathbf{R}^*_{22}}^{-1}(\mathbf{l}^2_\mathbf{n} - \mathbf{R}^*_{21}\mathbf{q}^1_\mathbf{n}) \tag{4.41}$$

Finally, the space time discontinuous integration scheme is implemented such discribed in algorithm 7.

Algorithm 7 DG time integration scheme for enforced/free displacement

Require: $\mathbf{R}$, $\mathbf{P}$, u_c, Initial conditions: $\mathbf{u}_0$, $\mathbf{v}_0$
  $v_c \leftarrow \dot{u_c}$
  $\mathbf{u}^-_0 \leftarrow \mathbf{u}_0$
  $\mathbf{v}^-_0 \leftarrow \mathbf{v}_0$
  $\mathbf{R}^* \leftarrow \mathbf{P}\mathbf{R}^t\mathbf{P}$
  Enforced displacement phase :
  for $n = 1$ **to** N_{T_c} **do**
    $\mathbf{l}_n \leftarrow \mathbf{l_n}(\mathbf{u^-_{n-1}}, \mathbf{v^-_{n-1}})$
    $\mathbf{l}^*_n \leftarrow \mathbf{P}\mathbf{l_n}$
    $\mathbf{q}^1_n \leftarrow \begin{pmatrix} u_c(t^+_{n-1}) & u_c(t^-_n) & v_c(t^+_{n-1}) & v_c(t^-_n) \end{pmatrix}^T$
    $\mathbf{q}^2_n \leftarrow {\mathbf{R}^*_{22}}^{-1}(\mathbf{l}^2_n - \mathbf{R}^*_{21}\mathbf{q}^1_n)$
    $\mathbf{q}^*_n \leftarrow \begin{pmatrix} \mathbf{q}^1_n & \mathbf{q}^2_n \end{pmatrix}^T$
    $\mathbf{q}_n \leftarrow \mathbf{P}^t\mathbf{q}^*_n = \begin{pmatrix} \mathbf{u}^+_{n-1} & \mathbf{u}^-_n & \mathbf{v}^+_{n-1} & \mathbf{v}^-_n \end{pmatrix}^T$
  end for
  Free displacement phase :
  for $n = N_{T_c}$ **to** N **do**
    $\mathbf{l}_n \leftarrow \mathbf{l}_n(u^-_{n-1}, v^-_{n-1})$
    $\mathbf{q}_n \leftarrow \mathbf{R}^{-1}\mathbf{l}_n$
  end for

4.2.3 Results

We consider the rod model already used in 3.2.3. Results are plotted at time t^+_n for $\Delta t = 10^{-2}$ s and for $\Delta x = L/30$ m. One can notice in figure 4.4 that DGM pro-

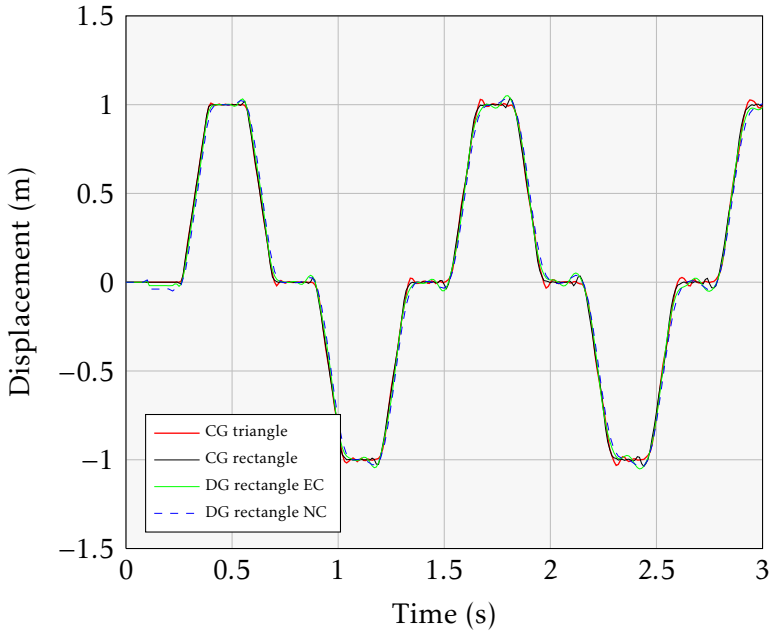

Figure 4.4: Response at $x = \frac{L}{2}$ to a ramp entry

vides a solution where high frequency oscillations are removed comparated to CGM and equivalent Newmark methods. This effect is even more visible when discontinuity is introduced in the enforced displacement as shown in figure 4.5. Also, the DG formulation provides access to both velocity and displacement

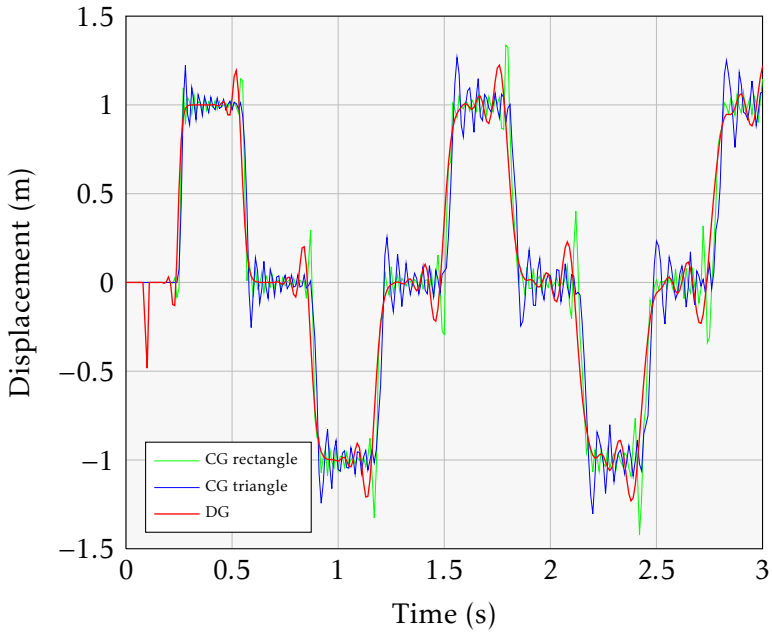

Figure 4.5: Response at $x = L/2$ to a ramp entry with an infinite slope

with the same linear approximation and is third order accurate. It is then more accurate than CGM mainly when discontinuous enforced displacement is used as depicted in figure 4.6. It is also worth noticing the large unexpected

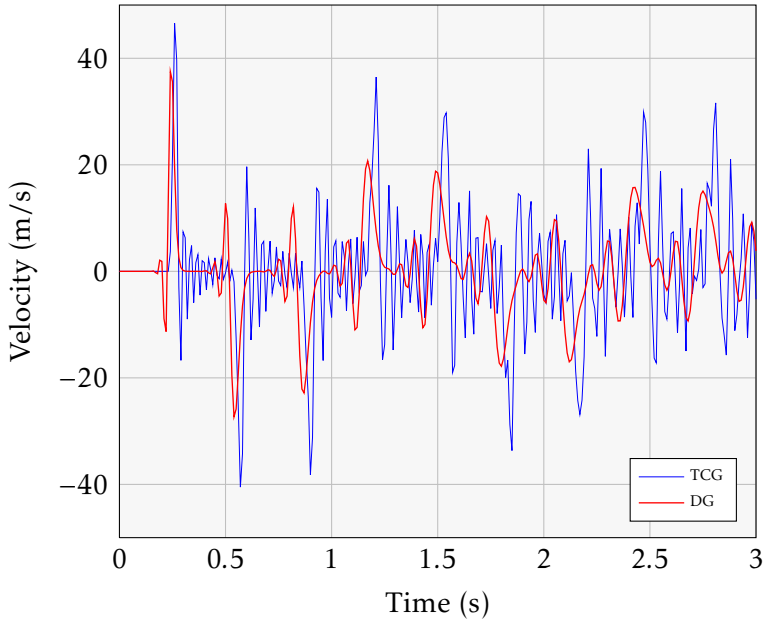

Figure 4.6: Response at $x = L/2$ to a ramp entry with an infinite slope

pertubation in the displacement in the DGM while the initial wave has not yet reach the middle point of the rod. These perturbations may be due to an error in the code or more likely to the use of rectangular elements in the DGM.

Conclusion

In this report, time integration using finite elements has been investigated. First, it has been shown that continuous Galerkin finite element methods using linear basis functions could be related to central differences Newmark methods. Moreover the use of quadratic basis functions provides a great gain of accuracy. However, these formulations are less efficient when nonlinearities are introduced. That is why attention was paid to discontinuous Galerkin finite element methods.

As it has been foreseen, the type of elements used in space-time finite elements method seems to be a sensitive choice. Indeed, muliplices always lead to a numerical model where information propagates at infinite velocity through the system while use of simplices tends to avoid this phenomenon.

Few investigations remain to be conducted. It would be of high interest to search and develop an error estimate for both discontinuous and continuous Galerkin methods in order to quantitatively compare them. Effects of higher order basis functions on the accuracy of the method and formulations with several fields are also possible future roads of investigation. Ultimately, purely periodic motions as proposed in [25] could be explored by weakly enforcing the periodicity conditions in time.

References

[1] L. Adélaïde. "Méthode des éléments finis espace-temps : adaptation du maillage en cours d'évolution du contact". PhD Thesis. Université Montpellier II, 2001 (pp. 25, 26, 31).
oai:tel.archives-ouvertes.fr:tel-00609164.

[2] J. Argyris and D. Scharpf. "Finite elements in time and space". *Nuclear Engineering and Design* 10.4 (1969), pp. 456–464 (p. 25).
DOI: 10.1016/0029-5493(69)90081-8.

[3] D. Arnold, F. Brezzi, B. Cockburn, and L. Marini. "Unified Analysis of Discontinuous Galerkin Methods for Elliptic Problems". *SIAM Journal on Numerical Analysis* 39.5 (2002), pp. 1749–1779 (pp. 38, 39).
DOI: 10.1137/S0036142901384162.

[4] P. Boisse, P. Bussy, and P. Ladeveze. "A new approach in nonlinear mechanics: The large time increment method". *International Journal for Numericla Methods in Engineering* 29.3 (1990), pp. 647–663.
DOI: 10.1002/nme.1620290312.

[5] O. Bokhove and J. Van der Vegt. *Introduction to (dis)continuous Galerkin finite element methods*. Numerical Analysis and Computational Mechanics. Department of Applied Mathematics, University of Twente, 2005 (p. 38).

[6] A-S. Bonnet-Ben Dhia and J-F. Mercier. *Ondes dans les milieux continus*. Ecole Centrale Paris, 2010.

[7] F. Chiba and T. Kako. "Stability and error analyses by energy estimate for Newmark's method". *National Institute for Fusion Science* 17-18.40 (1999), pp. 82–91.

[8] J. Chung, E-H. Cho, and K. Choi. "A priori error estimator of the generalized α-method for structural dynamics". *International Journal for Numerical Methods in Engineering* 57.4 (2003), pp. 537–554.
DOI: 10.1002/nme.688.

[9] J. Chung and G. M. Hulbert. "A Time Integration Algorithm for Structural Dynamics With Improved Numerical Dissipation: The Generalized-α Method". *Journal of Applied Mechanics* 60.2 (1993), pp. 371–375.
DOI: 10.1115/1.2900803.

[10] D. French. "A space-time finite element method for the wave equation". *Computer Methods in Applied Mechanics and Engineering* 107.1-2 (1993), pp. 145–157 (p. 37).
DOI: 10.1016/0045-7825(93)90172-T.

[11] T. Hughes and G. Hulbert. "Space-time finite element methods for elastodynamics: Formulations and error estimates". *Computer Methods in Applied Mechanics and Engineering* 66.3 (1988), pp. 339–363 (p. 37).
DOI: 10.1016/0045-7825(88)90006-0.

[12] T. Hughes, K. Pister, and R. Taylor. "Implicit-explicit finite elements in nonlinear transient analysis". *Computer Methods in Applied Mechanics and Engineering* 17-18.Part 1 (1979), pp. 159–182.
DOI: 10.1016/0045-7825(79)90086-0.

[13] G. Hulbert. "Time finite element methods for structural dynamics". *International Journal for Numerical Methods in Engineering* 33.2 (1992), pp. 307–331 (p. 37).
DOI: 10.1002/nme.1620330206.

[14] G. Hulbert and T. Hughes. "Space-time finite element methods for second-order hyperbolic equations". *Computer Methods in Applied Mechanics and Engineering* 84.3 (1990), pp. 327–348 (p. 37).
DOI: 10.1016/0045-7825(90)90082-W.

[15] A. Idesman. "Solution of linear elastodynamics problems with space-time finite elements on structured and unstructured meshes". *Computer Methods in Applied Mechanics and Engineering* 196.9-12 (2007), pp. 1787–1815 (p. 26).
DOI: 10.1016/j.cma.2006.09.019.

[16] A. Idesman, R. Niekamp, and E. Stein. "Continuous and discontinuous Galerkin methods with finite elements in space and time for parallel computing of viscoelastic deformation". *Computer Methods in Applied Mechanics and Engineering* 190.8-10 (2000), pp. 1049–1063 (p. 25).
DOI: 10.1016/S0045-7825(99)00463-6.

[17] C. Johnson. "Discontinuous Galerkin finite element methods for second order hyperbolic problems". *Computer Methods in Applied Mechanics and Engineering* 107.1-2 (1993), pp. 117–129 (p. 37).
DOI: 10.1016/0045-7825(93)90170-3.

[18] F. Jourdan. "Dynamique des structures et lois d'interface". HDR. Université Montpellier II, 2006 (pp. 25, 31).
oai:tel.archives-ouvertes.fr:tel-00583223.

[19] Y. Ke. "A unified solution for longitudinal wave propagation in an elastic rod". *Journal of Sound and Vibration* 314.1-2 (2008), pp. 307–329.
DOI: 10.1016/j.jsv.2008.01.007.

[20] R. Kirby and G. Karniadakis. "Selecting the numerical flux in discontinuous Galerkin methods for diffusion problems". *J. Sci. Comput.* 22-23 (1 June 2005), pp. 385–411 (p. 38).
DOI: 10.1007/s10915-004-4145-5.

[21] J. Melenk and I. Babuska. "The partition of unity finite element method: Basic theory and applications". *Computer Methods in Applied Mechanics and Engineering* 139.1-4 (1996), pp. 289–314.
DOI: 10.1016/S0045-7825(96)01087-0.

[22] A. Metrikine and A. Vrouwenvelder. *Dynamics of Strucutures - Wave Dynamics*. CT4140 vol. 2. Delft University of Technology, 2009.

[23] D. Pepper and J. Heinrich. *The finite element method: basic concepts and applications*. Computational and physical processes in mechanics and thermal sciences 1. Hemisphere Pub. Corp., 1992.

[24] J. Réthoré, A. Gravouil, and A. Combescure. "A combined space-time extended finite element method". *International Journal for Numerical Methods in Engineering* 64.2 (2005), pp. 260–284.
DOI: 10.1002/nme.1368.

[25] K. Vemaganti. "Discontinuous Galerkin method for peiodic boundary methods". *Numerical Methods for Partial Differential Equations* 23.3 (2007), pp. 587–596 (p. 49).
DOI: 10.1002/num.20191.

[26] N-E. Wiberg and X. Li. "Adaptive finite element procedures for linear and non-linear dynamics". *International Journal for Numerical Methods in Engineering* 46.10 (1999), pp. 1781–1802 (pp. 37, 39, 44).
DOI: 10.1002/(SICI)1097-0207(19991210)46:10<1781::AID-NME724>3.0.CO;2-7.